NSG-1136

SOLIDIFICATION UNDER ZERO GRAVITY- A LONG DURATION EXPOSURE FACILITY (LDEF) EXPERIMENT FOR AN EARLY SPACE SHUTTLE MISSION

BY

JOHN A. BAILEY, B.Sc., Ph.D., F.I.M.

DEPARTMENT OF MECHANICAL AND AEROSPACE ENGINEERING
NORTH CAROLINA STATE UNIVERSITY
RALEIGH, NORTH CAROLINA 27607

SOLIDIFICATION UNDER ZERO GRAVITY - A LONG DURATION EXPOSURE FACILITY (LDEF) EXPERIMENT FOR AN EARLY SPACE SHUTTLE MISSION

Final Report to National Aeronautics and Space Administration Grant NSG 1136

Submitted to

Space Applications and Technology Division
National Aeronautics and Space Administration,
Langley-Hampton, Virginia 23665

by

John A. Bailey, B.Sc., Ph.D., F.I.M.

Department of Mechanical and Aerospace Engineering
North Carolina State University
Raleigh, North Carolina 27607

ABSTRACT

The preliminary design of two series of simple experiments the objectives of which are to determine the effect of an absence of gravity on (i) the general morphology of the structure, (ii) location of ullage space, and (iii) magnitude of surface tension driven convection, during the solidification of several metallic and non-metallic systems is described. Details of the investigative approach, experimental procedure, experimental hardware, data reduction and analysis, and anticipated results are given. In addition a work plan and cost analysis is provided.

TABLE OF CONTENTS

TABLE OF CONTENTS (Cont.)

LIST OF SYMBOLS

Cp	Specific heat, cal/gm°C
$\dot{g}$	Heat rate, cal/hr
g	Acceleration due to gravity, found in Bond Number
K	Thermal conductivity, watts/cm°C
L	Length, cm
L_T	Latent heat of fusion, cal/gm
q	Heat flux, cal/cm^2-hr
s	Solid liquid interface position, cm
T	Temperature, °C
t	Time, usually hr
v	Kinematic viscosity, cm^2/sec
α	Thermal diffusivity, cm^2/sec
β	Volumetric coefficient of expansion, 1/°C
δ	Thermal boundary, cm
ρ	Density, gm/cm^3
σ	Surface tension, dynes/cm

1. SCOPE

The present report is a statement of work carried out under National Aeronautics and Space Administration Grant NSG 1136 entitled "Long Duration Exposure Facility (LDEF) Experiments for Early Space Shuttle Missions" and covers the working period January 15, 1975 to May 14, 1976.

2. INTRODUCTION

Approximately two years ago, several experiments concerning the effects of a space environment on the melting-freezing behavior and frictional characteristics of materials were proposed by the principal investigator. These experiments formed a portion of a total of seventeen suggested for possible conduct aboard the early flights of the proposed space shuttle. A brief description of the experiments was given in a document entitled, "Phase A Planning Document", prepared by Dr. J. J. Wortman of the Engineering Division of the Research Triangle Institute for the National Aeronautics and Space Administration.

Tentative approval of the experiments led to the award by the National Aeronautics and Space Administration of a one year contract beginning on January 15, 1975 for the sum of $9,998.58, for the generation of background information and data of value in the future design, construction and testing of the aforementioned experiments.

More recent screening of candidate experiments by the National Aeronautics and Space Administration has led to the selection of a portion of the proposed experiments concerned with a study of the melting-freezing behavior of materials in a space environment as being feasible for conduct aboard an early space shuttle flight, where technical simplicity is essential. It was decided that the proposed experiment concerning the frictional

characteristics of materials should be removed from further consideration until a later date because of its technical complexity.

A presentation of the objectives, investigative approach, anticipated results and implications of the proposed experiments concerned with a study of the melting-freezing behavior of materials was given to Dr. Smiley at NASA Headquarters, Washington, D. C. on March 6, 1975 and to LDEF Project personnel at NASA Langley Research Center, Hampton, Virginia on May 20, 1975. Subsequently, the principal investigator was requested to submit a proposal to allow final selection of the first LDEF experiments.

The work described in this report is concerned with the generation of information necessary for the successful design of the proposed experimental package. A brief summary of previous work and objectives of the proposed experiments is given in Sections 3 and 4, respectively. The investigative approach, experimental materials, and experimental hardware are described in Sections 5, 6 and 7, respectively. Data analysis and anticipated results are described in Sections 8 and 9, respectively. Finally, a detailed work plan is given in Section 10.

3. PREVIOUS WORK

Interest in the solidification behavior of materials in a ZERO-G environment has developed rapidly during the past several years. This interest was generated largely by the success of the Apollo and Skylab missions which provided the capability for performing unique experiments in a space environment. Solidification in a ZERO-G environment occurs with the absence of both mechanical vibration and buoyancy driven convection. This can lead to the generation of components with improved mechanical and physical properties.

At the present time most of the work conducted has been of an exploratory nature and concerned primarily with the development of systems which can be used for studying the melting and freezing behavior of materials over a wide range of experimental conditions. Experiments have been conducted concerning the solidification of pure materials, immiscible alloys, and eutectics, the fluid dynamics of liquid droplets, containerless melting and the growth of single crystals. The important aspects of these experiments are given in Table I.

Much of the previous work concerning the solidification of materials in a ZERO-G environment has been carried out aboard Skylab using the M512 processing facility. This facility uses the Westinghouse M518 multipurpose resistance heating furnace and electron beam gun. The complete electrical resistance furnace consists of three major components namely; the furnace, the control package and experimental cartridges which contain the test materials. The furnace design is such that constant temperatures up to 1000°C can be maintained at the hot end. In addition, a passive heat sink is provided at the cold end of the furnace so that temperature gradients can be established. The furnace can accommodate three cartridge test samples for heating periods up to 64 hours at a power level of 144 watts. In addition, an electron gun is used to provide a high temperature point heat source.

The principal conclusions which may be drawn from a comparison of the solidification behavior of materials in a ZERO-G and NORMAL-(one) G environment are, that for a ZERO-G environment:

1. The structure is free from effects associated with buoyancy driven convection.

2. Segregation of impurities is reduced producing a more homogeneous microstructure.

3. Segregation of phases in immiscible alloys is reduced producing a more homogeneous microstructure. However, segregation can occur slowly through coalescence.

4. The heterogeneous nucleation rate is reduced because of reduced segregation.

5 Supercooling is greater because of the more uniform distribution of impurities and the absence of vibration.

6. There is an increase in the amount of porosity because trapped gases cannot escape from the melt.

7. Capilliary fluid motion can be appreciable.

8. Melt contamination is less in containerless melting.

4. OBJECTIVES

The environment of the orbiting LDEF provides a very unique opportunity for studying phenomena associated with the behavior of materials under conditions which previously were unobtainable. Perhaps one of the most interesting and important natural phenomena is that of solidification which is associated with the liquid⇄solid phase change.

The basic objective of the proposed experiment is to determine whether or not solidification of materials (metals and nonmetals) in a ZERO-G environment is different from that occurring in a ONE-G environment. In particular, the absence of gravity on (i) the general morphology of the structure, (ii) the location of ullage space, and (iii) the magnitude of surface tension driven convection will be studied.

TABLE 1. Summary of Experiments Performed in a Zero Gravity Environment

Experiment	Purpose of Investigation	Facility	Material System	Experimental Conditions	Results
Solidification of immiscible alloys [References 1, 2]	To determine effects of zero gravity on segregation	M518 Multi-purpose Furnace [Reference 12]	1*. Au(78.85) - Ge (23.15) 2*. Pb(45.05) - Zn (45.06) - Sn (9.8) 3*. Pb(70.2) - Sn (14.8) - In (15.0)	Systems (1) and (2) were heated to 720°C, held at temperature for four hours then allowed to cool. System (3) was partially melted and held under a fixed temperature gradient then cooled.	In general, more homogeneous microstructures were obtained compared with similar samples solidified under normal gravitational conditions.
Solidification of NaCl - NaF eutectic [Reference 3, 4]	To determine effect of zero gravity on lamellar microstructure of eutectic	M518 Multi-purpose Furnace [Reference 12]	NaCl(21) - NaF (79) eutectic composition	Melt was solidified unidirectionally under a temperature gradient of 50°C/cm.	Continuous NaF fibers were produced in a fault free NaCl matrix. Fibers were aligned parallel to direction of solidification. Optical properties were superior to material solidified under normal gravitational conditions.

TABLE 1. (Cont.)

Formation of spheres [References 5, 6]	To study the fluid dynamics of molten droplets in zero gravity	M518 Multipurpose Furnace [Reference 12]	1. Ni(88) - Sn(12) eutectic alloy 2. Ni(99) - Ag(1) monotectic alloy	Materials were heated with an electron beam in vacuum and melted with absence of container.	In general, solidification occurs initially at surface and progresses radially inwards. Some surface tension driven fluid flow at surface observed. System (1) showed excessive undercooling. Some differences in shrinkage and porosity were observed when compared with material solidified under normal gravitational conditions. System (2) gave an almost perfect silver coated sphere.
Melting of Metals Proposed Experiment [Reference]	To study the fluid dynamics of molten materials in zero gravity	M518 Multipurpose Furnace [Reference 12]	1. Al Alloy 2219 2. Stainless Steel 321 3. Tantalum	Machined discs of materials will be rotated and heated with an electron beam in vacuum to form circular liquid bead.	It is anticipated that more perfectly shaped beads can be formed.

TABLE 1. (Cont.)

Electromagnetic Containerless Melting (Proposed Experiment) [References 7, 8]	To study the effects of solidification under zero gravity on microstructure	Electromagnetic Levitation Heating Unit	1. Intermetallic Compounds 2. Cermets 3. Transition metal carbides and nitrides. 4. Glasses	Materials will be melted using levitation heating unit with various shaped coils.	It is anticipated that contaminant free, homogeneous spherical beads can be produced having a very low density. It is hoped to show that a greater range of materials can be tested because of the extremely low forces required to maintain bead stability.
Solidification of Eutectics [References 9, 6, 10, 5]	To study the effects of solidification under zero gravity or microstructural defects	M518 Multipurpose Furnace [Reference 12]	Al(67) - Cu(33)	Experiments conducted under conditions of unidirectional solidification to obtain lamellar structure.	Lamellar spacing of Al and Cu Al_2 plates and fault density were measured. Little differences as compared with same material solidified under normal gravitational conditions.
Growth of Single Crystals (Proposed Experiment) [Reference 11]	To attempt to reduce microstructural defects by solidification under zero gravity	M518 Multipurpose Furnace [Reference 12]	1. Pure Ag 2. Ag doped with Ge 3. Cu-Au alloys	Single Crystals to be grown in two types of crucible.	It is hoped that absence of gravity will produce crystals of low defect density with improved electrical properties.

For gravitational environments in the range from ZERO-G to ONE-G interatomic forces in materials are greater than the gravitational forces to the point where differences in the mechanisms of solidification and fine scale structure would not be anticipated. However, it is believed that a reduction in the magnitude of the gravitational forces can lead to changes in the location of the ullage space and the onset of surface tension driven convection. The ullage space is that space which must be provided to allow for contractions and expansions of materials during the melting/freezing process. In a ZERO-G environment there will be an absence of natural convection because of the lack of buoyancy forces. However, convection driven by surface tension forces could be appreciable. Convection driven by surface tension forces is known as Marangoni flow.

The proposed experiments, although of necessity technically simple, will provide a very unique opportunity to generate qualitative and quantitative information which will lead to an advancement in our understanding of the basic principles of solidification and provide a firm basis for the development of more sophisticated experiments at a later date. It is believed also that the aforementioned experiments can provide data which is of more immediate and direct practical value. Recently, cooling/heating devices (thermal capacitors) have been developed based on the use of an encapsulated material (PCM) which is forced to undergo a phase change (solid⇄liquid). The device absorbs heat from an external medium when the phase change material (PCM) melts and rejects heat to the medium when the phase change material solidifies. The heat absorbed or rejected is, of course, the latent heat of fusion of the phase change material.

Thermal capacitors have been used for temperature control and heat storage on the Lunar Roving Vehicle (LRV), Skylab I and Apollo's 15, 16 and

17. However, it is believed that potential problems may develop if solidification in the space environment is not controlled. For example, if the ullage space forms adjacent to the channel carrying the externally circulating medium then heat transfer will be seriously impaired and the efficiency of the capacitor reduced. Under normal gravitational conditions (ONE-G) the position of the ullage space can be controlled by suitable orientation of the capacitor. However, such control is not possible in a zero gravity environment. In the absence of gravity it is important to know how and where the ullage space forms so that future capacitor designs can be improved. Similarly, capacitor performance may be changed radically should surface tension driven convection become an important mode of heat transfer. Most thermal capacitor designs are based on conduction models of the heat transfer process. Clearly, the proposed experiments could provide valuable information of direct use in the design of thermal capacitors for future space missions.

In the proposed experiments it is hoped to show that some control over the location of the ullage space can be established by selection of the appropriate relative interfacial energy between the test material (liquid) and container. It is hoped also to show that surface tension driven convection can be generated and controlled by control of the temperature gradient and hence local surface tension along an interface (liquid-vapor).

5. INVESTIGATIVE APPROACH

5.1 Concepts of Experiments

It is proposed to conduct two different but related series of experiments. One experiment will be concerned with an investigation of the

general morphology of the structure produced by solidification of a liquid. The other experiment will be concerned with an investigation of the magnitude of surface tension driven convection. Both experiments will be conducted, of course, in a zero gravity evnvironment. The schematic arrangement for the experiments is given in Figure 1.

5.1.1 General Morphology Studies

In the first series of experiments a small cylindrical sample of each test material with a volume in the range from one to three cubic centimeters and with a height to diameter ratio of approximately unity will be press-fitted into a lined, stainless steel container. The containers will be filled with argon at normal atmospheric pressure and sealed. The size of the containers will be such that there will be approximately seventy percent ullage. The containers will be attached securely to wire wound resistance heating units (furnaces). The container assembly is illustrated schematically in Figure 2. The capability of the units will be such that sufficient heat can be produced to melt the sample. For testing low melting point translucent materials, the containers will be made from a high melting point transparent plastic so that visual observation of the total morphology of the structure can be made after solidification. Heating will be from "below" so that stability will be maintained until the test sample is completely melted.

The linings of the container and/or actual test materials will be selected to meet two broad requirements, namely; (1) test material wets container (low relative interfacial energy), and (2) test material does not wet container (high relative interfacial energy). Two identical cells for each material will be made. This scheme enables the effects of variations in the relative interfacial energy between container and test material

on the general morphology and location of ullage space to be studied. The materials systems which may serve as potential candidates for the proposed experiments are discussed in Section 6 of this report.

5.1.2 Convection Studies

In the second series of experiments small samples of each test material will again be press-fitted into lined stainless steel containers and sealed under an atmosphere of argon as in the previous series of experiments. However, here the ullage space will be reduced to approximately 25% and the diameter to height ratio of the cylinder will be of the order of two in order to provide a large solid (liquid)-vapor interface. In addition, a small platinum wire heating element will protrude from one end of the cylinder into the ullage space. The active (hot) end of the element will be located approximately 5mm above the solid surface of test sample. This is illustrated schematically in Figure 3. The materials finally selected for the studies in Section 5.1.1 described above will be used in this series of experiments. However, two identical cells for each material will be made. It is hoped that with this scheme investigation of the effects of variations in interface tension produced by interface temperature gradients on convection can be studied for liquid-vapor interfaces.

5.2 Experimental Procedure

The experimental procedures to be used are particularly simple and therefore ideally suitable for conduct aboard the first several flights of the space shuttle.

For the first series of experiments [(5.1.1) above] the test materials will be heated from "below" to produce complete melting. The capsule will be designed such that the solid-liquid interface will originate

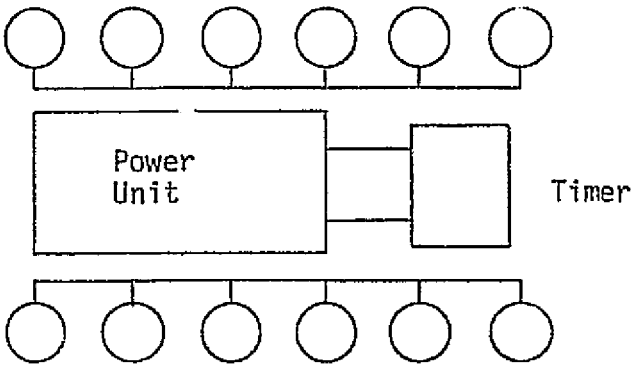

FIGURE 1. Experimental Arrangment (schematic).

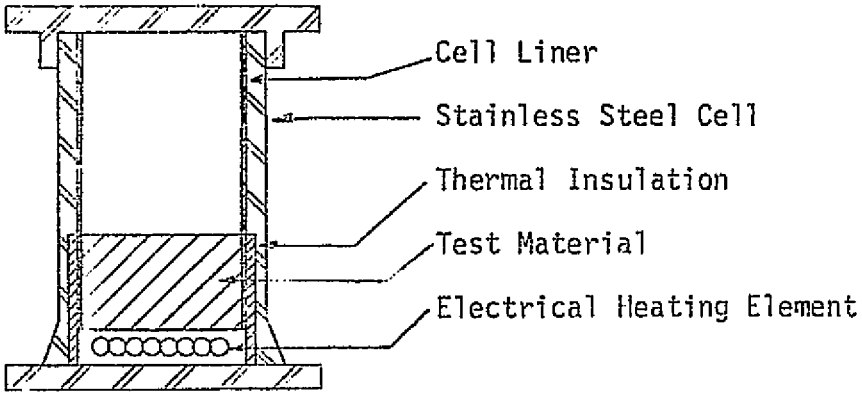

FIGURE 2. Test Cell (i) (schematic section).

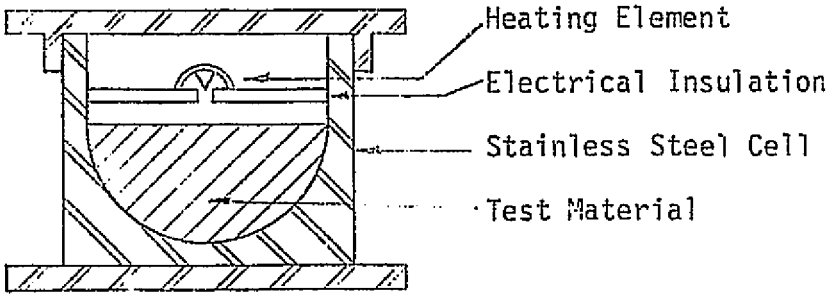

FIGURE 3 Test Cell (ii) (schematic section).

adjacent to the heat source and move perpendicular to the axis of the capsule. In this way material stability will be maintained until the solid is completely melted. Each sample will be held in the liquid state for similar prescribed periods of time then allowed to cool to ambient temperature. For the second series of experiments [(5.1.2) above] a current will be passed through the platinum wire heating element to produce radiant heating of the center most portion of the "upper" surface of the test material. Each sample will be heated for prescribed but different periods of time then allowed to cool to ambient temperature. It is important to state here that these test samples will not be melted completely. The unmelted material will serve to stabilize the melted material because of the surface tension forces generated at the solid-liquid interface.

In the initial experimental design it was proposed that power consumptions and temperature distributions within the test cells be measured and recorded continuously as a function of time during the real time life of the experiment. However, recent restrictions have led to the elimination of this aspect of the program. Thus, in flight quantitative data will not be generated. The experimental results will be generated from post flight sample characterization and will be described in Section 8 of this report. Assistance from the Shuttle crew will not be needed. However, assistance from Ground Support personnel will be required for delivery, installation and retrieval of the experimental package.

6. EXPERIMENTAL MATERIALS SELECTION

In the initial proposal for the experimental package it was intended to select materials from systems possessing widely different physical and

chemical characteristics so that a comprehensive broad based program of activity could be established. The tentative systems identified included low melting point pure metals, low melting point immiscible alloys, low melting point eutectiferrous alloys, pure paraffin hydrocarbons and paraffin hydrocarbon mixtures. Recently, it was suggested that the scope of the proposed activity be reduced to fit within the revised objectives of the LDEF mission. Accordingly, it is now proposed to select low melting point pure metals and either pure paraffin hydrocarbons or pure fatty acids as the systems for investigation. However, physical and thermal property data will be given where possible for all of the material systems identified initially. The melting points of the materials will be kept in the approximate range from 40°C to 600°C to keep power requirements and design difficulties at a minimum.

Table II contains a list of pure metals of potential interest. Although gold and silver have melting points considerably in excess of 600°C they have been included as potential candidate test materials because of their noble characteristics. Their use could avoid possible problems associated with oxidation during test. Table III contains a list of immiscible alloy systems. The Lead-Zinc and Aluminum-Thallium systems represent the most promising candidates. The remaining systems involve reactive metals which may prove hazardous. Unfortunately, thermal property data for these materials is not available. However, phase diagrams for these systems are given in Figures 4, 5 and 6. Table IV contains thermal property data for a number of low melting point metallic eutectic systems. Tables V and VI contain thermal property data for selected pure paraffin hydrocarbons and other organic compounds, respectively. Table VII contains thermal property data of selected fatty acids. Table VIII contains a list of

possible organic eutectic systems. Unfortunately, thermal property data for these systems is not available.

It is intended to select ultimately materials which will wet the containment capsule (low relative interfacial energy) and materials which will not wet the containment capsule (high relative interfacial energy). At the present time data concerning the relative interfacial energies and wetting characteristics of those test and containment materials identified as being potential candidates for the proposed experiments is not available. It is proposed that generation of this data be undertaken as the initial step in the final design program which will be undertaken at a later date. Similarly, thermal property data for the immiscible alloy and organic eutectic systems will be determined at a later date.

7. EXPERIMENTAL HARDWARE

7.1 Physical Characteristics

The experimental package will consist of twelve test cells as described in a previous section, a battery power pack, and timer to initiate the experiment. The package will be rectangular in section measuring approximately 50 cm x 76 cm x 15 cm (0.057 m^3) and weigh approximately 8.1 kg. The power system will consist of a DC battery pack to furnish power for melting the test samples and driving the timer module. Data recording systems are not required with the revised experimental profile.

The experimental package will be designed such that it will neither produce, nor be susceptible to degradation through electromagnetic interference contamination, acoustic radiation and mechanical vibration over the levels anticipated during ground handling, launch, space exposure and recovery. The only active components in the experimental package are the

TABLE II. Thermal Property Data for Pure Metals [13].

Metal	Melting Point (°C)	Latent Heat (Cal/gm)	Specific Heat (Cal/gm °C)	Density (gm/cc)	Thermal Conductivity (watt/cm °C)
Aluminum (Al)	660.2	95.0	0.215	2.70	2.370
Antimony (Sb)	630.5	38.5	0.050	6.70	0.185
Bismuth (Bi)	271.5	12.4	0.030	9.80	0.084
Cadmium (Cd)	320.9	13.2	0.055	8.64	0.930
Gold (Au)	1063.0	15.0	0.031	19.30	3.150
Lead (Pb)	327.4	11.68	0.031	11.68	0.346
Magnesium (Mg)	650.0	88.0	0.243	1.74	1.590
Selenium (Se)	220.0	16.0	0.077	-	0.005
Silver (Ag)	960.8	26.5	0.057	10.50	4.270
Tin (Sn)	237.1	14.1	0.054	7.30	0.640
Zinc (Zn)	419.4	27.0	0.093	7.14	1.150

TABLE III. Immiscible Alloy Systems [13].

System	Immiscibility Gap Temperature Range Estimated (°C)	Freezing Point (°C)	Composition (weight %)
Lead-Zinc (Pb - Sn)	420 - 800	325	A wide range of compositions can be used. Varying chemical comrosition varies immiscibility gap.
Aluminum-Thallium (Al - Tl)	660 - 950	311	
Aluminum-Potassium (Al - K)	660 - 900	63	
Aluminum-Cadmium (Al - Cd)	650 - 950	320	
Magnessium-Sodium (Mg - Na)	650 - 950	97	
Potassium-Magnesium (K - Mg)	650 - 950	64	

TABLE IV. Thermal Property Data for Eutectic Alloys [13].

System	Melting Point (°C)	Density (gm/cc)	Specific Heat (cal/gm °C)	Thermal Conductivity (Watt/cm °C)	Composition (weight %)
Bismuth-Thallium (Bi - Tl)	185	10.81	0.031	0.015	Bi-48%, Tl-52%
Lead-Tin (Pb - Sn)	180	8.24	0.045	0.033	Pb-38%, Sn-62%
Tin-Cadmium (Sn - Cd)	175	7.70	0.055	0.045	Sn-67%, Cd-33%
Tin-Thallium (Sn - Tl)	170	9.20	0.044	0.033	Sn-57%, Tl-43%
Lead-Tin-Cadmium (Pb - Sn - Cd)	143	8.09	0.047	0.037	Pb-30%, Sn-51.2%, Cd-18.2%
Bismuth-Cadmium (Bi - Cd)	140	9.35	0.040	0.026	Bi-60%, Cd-40%
Bismuth-Tin (Bi - Sn)	140	8.63	0.040	0.019	Bi-58%, Sn-42%
Bismuth-Tin-Zinc (Bi - Sn - Zn)	130	8.55	0.042	0.021	Bi-56%, Sn-40%, Zn-4%
Bismuth-Lead (Bi - Pb)	125	10.30	0.030	0.012	Bi-55.6%, Pb 44.5%
Cadmium-Indium (Cd - In)	120	7.66	0.057	0.052	Cd-25%, In-75%

(Cont.)

TABLE IV. Thermal Property Data for Eutectic Alloys [13]. (Cont.)

Bismuth-Lead-Zinc (Bi - Pb - Zn)	118	10.20	0.032	0.013	Bi-55%, Pb-43%, Zn-2%
Tin-Indium (Sn - In)	117	7.24	0.056	0.045	Sn-48%, In-52%
Lead-Sodium-Lithium (Pb - Na - Li)	310	5.92	0.244	0.046	Pb-50%, Na-35%, Li-15%
Cadmium-Zinc (Cd - Zn)	270	8.47	0.063	0.074	Cd-82%, Zn-18%
Lead-Cadmium (Pb - Cd)	245	10.62	0.035	0.028	Pb-82%, Cd-18%
Lead-Antimony (Pb - Sb)	240	11.00	0.033	0.020	Pb-89%, Sb-11%
Lead-Cadmium-Antimony (Pb - Cd - Sb)	236	10.50	0.036	0.030	Pb-79.7%, Cd-17.7%, Sb-2.6%
Lead-Sodium-Lithium (Pb - Na - Li)	234	8.83	0.174	0.028	Pb-79%, Na-5%, Li-16%
Lead-Lithium (Pb - Li)	230	9.23	0.169	0.025	Pb-83%, Li-17%
Cadmium-Thallium (Cd - Tl)	205	11.35	0.035	0.030	Cd-17%, Tl-83%
Antimony-Thallium (Sb - Tl)	195	10.68	0.035	0.021	Sb-21%, Tl-79%

TABLE V. Thermal Property Data for Pure Paraffin Hydrocarbons [14].

Hydrocarbon	Formula	Melting Point (°C) Solid⇄Liquid	Transition Temperature (°C) Solid⇄Solid	Latent Heat (cal/gm)	Heat of Transition (cal/gm)	Density (gm/cc)		Specific Heat (cal/gm °C)	Thermal Conductivity (watts/cm °C)
						liquid	solid		
Pentacosane	$C_{25}H_{52}$	53.7	47.6	42.6	17.7	0.770	0.810	0.52	0.0015
Hexacosane	$C_{26}H_{54}$	56.4	53.3	38.8	21.0	0.773	0.811	0.53	0.0015
Heptacosane	$C_{27}H_{56}$	59.0	53.0	37.9	18.2	0.781	0.812	0.51	0.0015
Octacosane	$C_{28}H_{58}$	61.4	58.6	39.1	21.4	0.776	0.813	0.54	0.0015
Nonacosane	$C_{29}H_{60}$	63.7	58.2	38.6	17.3	0.780	0.814	0.55	0.0015
Triacontane	$C_{30}H_{62}$	65.8	62.0	60.0	None	0.781	0.814	0.55	0.0015
Hentriacontane	$C_{31}H_{64}$	67.9	65.0*	74.0*	11.2*	0.782	0.815	0.55	0.0015
Dotriacontane	$C_{32}H_{66}$	69.7	66.0*	75.5*	22.4*	0.782	0.816	0.55	0.0015
Tritriacontane	$C_{33}H_{68}$	71.4	70.0*	78.8*	24.6*	0.783	0.817	0.55	0.0015
Tetratricontane	$C_{34}H_{70}$	73.1	None	81.2*	None	0.784	0.818	0.56	0.0015
Pentatriacontane	$C_{35}H_{72}$	74.7	72.0*	82.4*	27.5*	0.785	0.820	0.57	0.0015
Hexatriacontane	$C_{36}H_{74}$	76.2	None	83.6*	None	0.786	0.821	0.58	0.0015
Heptatriacontane	$C_{37}H_{76}$	77.7	77.0*	84.1*	30.3*	0.787	0.822	0.58	0.0015
Octatriacontane	$C_{38}H_{78}$	79.0	None	86.0*	None	0.788	0.823	0.59	0.0015
Nonatriacontane	$C_{39}H_{80}$	80.3	82.0*	86.7*	32.2*	0.789	0.823	0.59	0.0015
Tetracontane	$C_{40}H_{82}$	81.5	None	87.2*	None	0.790	0.824	0.59	0.0015

*Extrapolated Data

TABLE VI . Other Organic Compounds.

Organic Compound	Formula	Melting Point (°C)
Pentaerythritol Tetraacetate	$C(CH_2OOCCH_3)_4$	83
*Acetamide	CH_3CONH_2	82
Diphenyl Carbonate	$(C_6H_5O)_2CO$	80
Naphthalene	$C_{10}H_8$	80
Diacetamide	$(CH_3CO)_2NH$	79
Ethylene Steurate	$(CH_3(CH_2)_{16}COOCH_2)_2$	79
Propionamide	$C_2H_5CONH_2$	79
Triacetamide	$(CH_3CO)_3N$	79
Glycerol Tribenzoate	$CH(CH_2OOCC_6H_5)_2OOC\cdot C_6H_5$	76
Phenyl Propionate	$C_3H_7COOC_6H_5$	76
Diphenyl Phthalate	$O\cdot C_6H_4(COOC_6H_5)_2$	73
1, 2 - Ethanediol Dibenzoate	$(C_6H_5COOCH_2)_2$	73
Biphenyl	$C_6H_5\cdot C_6H_5$	71
*Phenyl Benzoate	$C_6H_5COOC_6H_5$	71
Phenyl Ethylene Glycol	$C_6H_5CHOHCH_2OH$	69

*Supercools; has to be seeded periodically for cyclic melting-freezing.

TABLE VII Thermal Property Data for Selected Fatty Acids [14].

Fatty Acid	Formula	Melting Point (°C) Solid⇄Liquid	Latent Heat (Cal/gm)	Transition Temperature (°C) Solid⇄Solid	Heat of Transition (Cal/gm)	Specific Heat (Cal/gm °C)	
						Solid	Liquid
Pentadecanoic	$C_{15}H_{30}O_2$	52.5	42.5	12.0	-	0.467	0.531
Myristic	$C_{14}H_{28}O_2$	53.7	44.6	11.0	-	0.521	0.516
Margaric	$C_{17}H_{34}O_2$	61.5	45.2	25.2	14.6	0.506	0.560
Palmitic	$C_{16}H_{32}O_2$	62.8	44.3	23.2	-	0.492	0.542
Stearic	$C_{18}H_{36}O_2$	70.7	48.4	31.4	17.1	0.460	-
Arachidic	$C_{20}H_{40}O_2$	76.5	54.2	40.4	17.5	0.477	0.566
Tricosanoic	$C_{23}H_{46}O_2$	77.4	49.6	-	-	0.560	0.576
Behenic	$C_{22}H_{44}O_2$	80.2	55.1	47.8	18.2	0.485	0.556
Pentacosanoic	$C_{25}H_{50}O_2$	80.6	52.3	-	-	0.535	0.577
Lignoceric	$C_{24}H_{48}O_2$	83.1	57.2	-	-	0.467	0.586
Cerotic	$C_{26}H_{52}O_2$	87.4	59.2	-	-	0.479	0.571

TABLE VIII. Organic Eutectic Systems [1].

System	Melting Point (°C)	Composition (Weight %)
Benzamide-Benzoic Acid ($C_6H_5CONH_2$-C_6H_5COOH)	79	$C_6H_5CONH_2$-51.8%, C_6H_5COOH-48.2%
Urea-Benzoic Acid ($CO(NH_2)_2$-C_6H_5COOH	78	$CO(NH_2)_2$-33%, C_6H_5COOH-67%
Naphthalene-Hexachlorethane ($C_{10}H_{18}$-Cl_3CCCl_3)	57	$C_{10}H_{18}$-48.5%, Cl_3CCCl_3-51.5%
*Urea-Acetamide ($CO(NH_2)_2$-CH_3CONH_2)	53	$CO(NH_2)_2$-36.5%, CH_3CONH_2-63.5%
Phenanthrene-Naphthalene ($C_{14}H_{10}$-$C_{10}H_{18}$	51	$C_{14}H_{10}$-50.9%, $C_{10}H_{18}$-49.1%
Propionamide-Palmitic Acid (C_2H_5-$CONH_2$-$CH_3(CH_2)_{14}COOH$)	50	$C_2H_5CONH_2$-25.1%, $CH_3(CH_2)_{14}COOH$-74.9%

*Supercools has to be seeded periodically for cyclic melting-freezing.

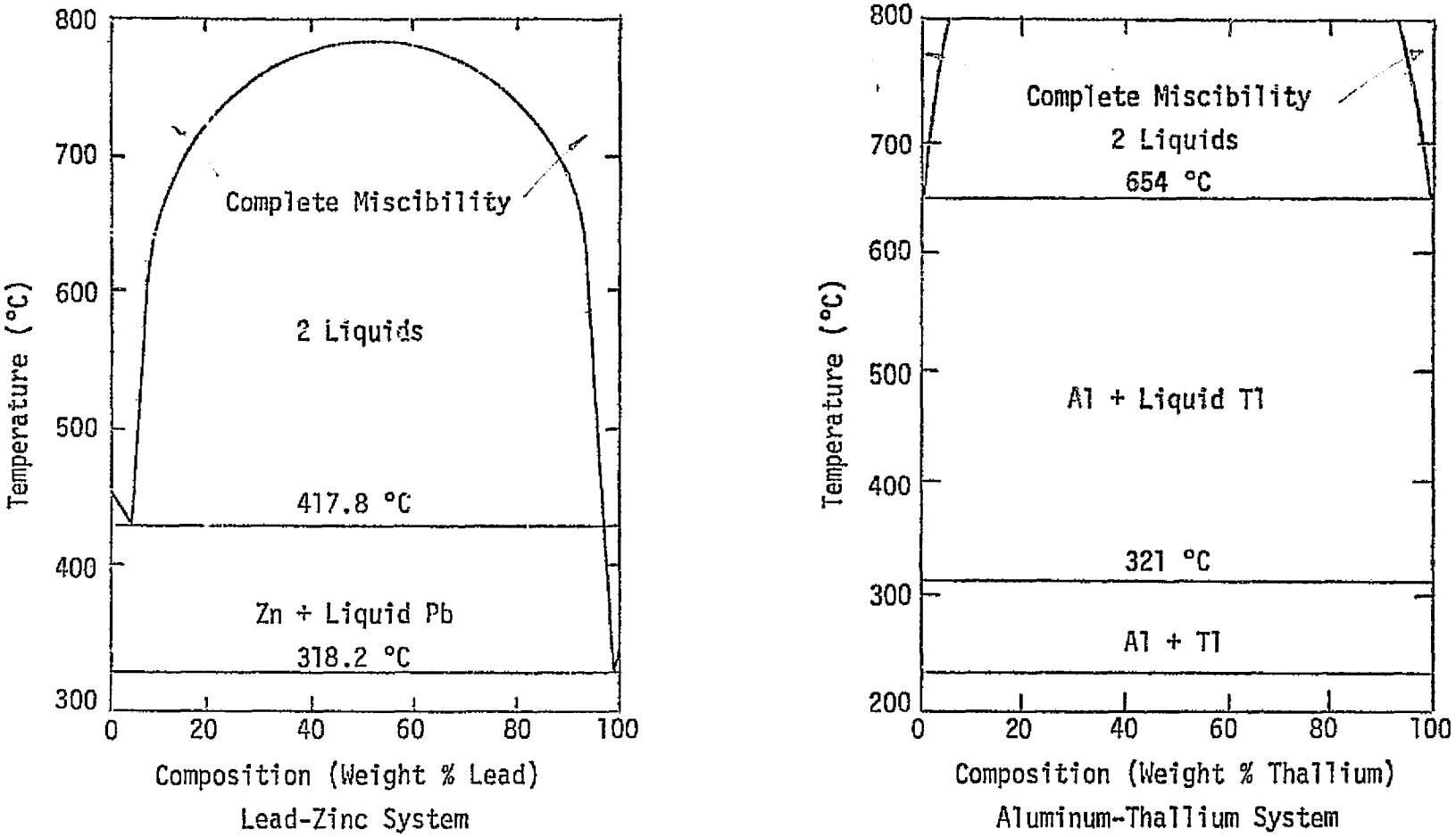

FIGURE 4 Phase Diagrams for the Lead-Zinc and Aluminum-Thallium Systems.

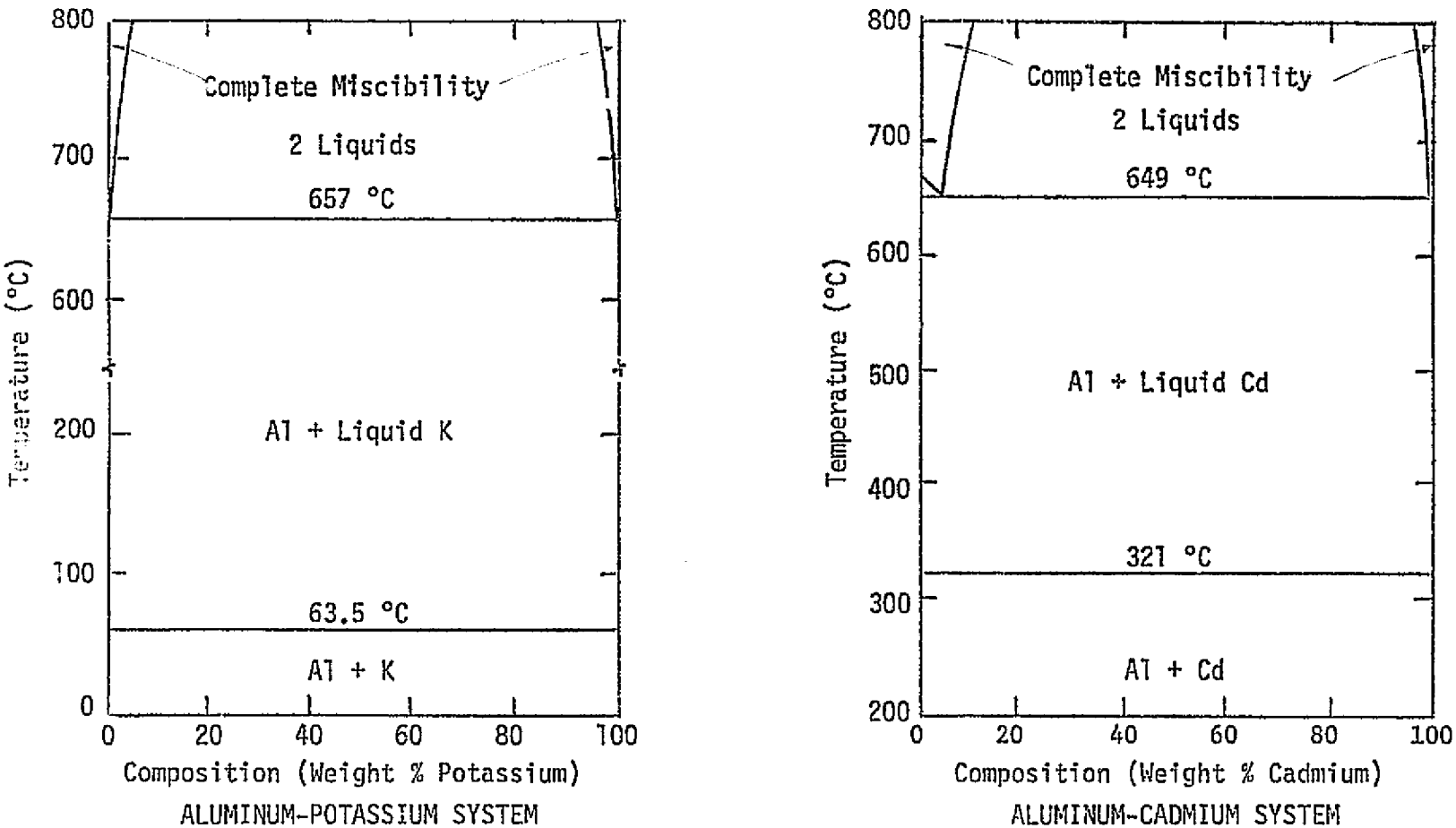

FIGURE 5 Phase Diagrams for the Aluminum-Potassium and Aluminum-Cadmium Systems.

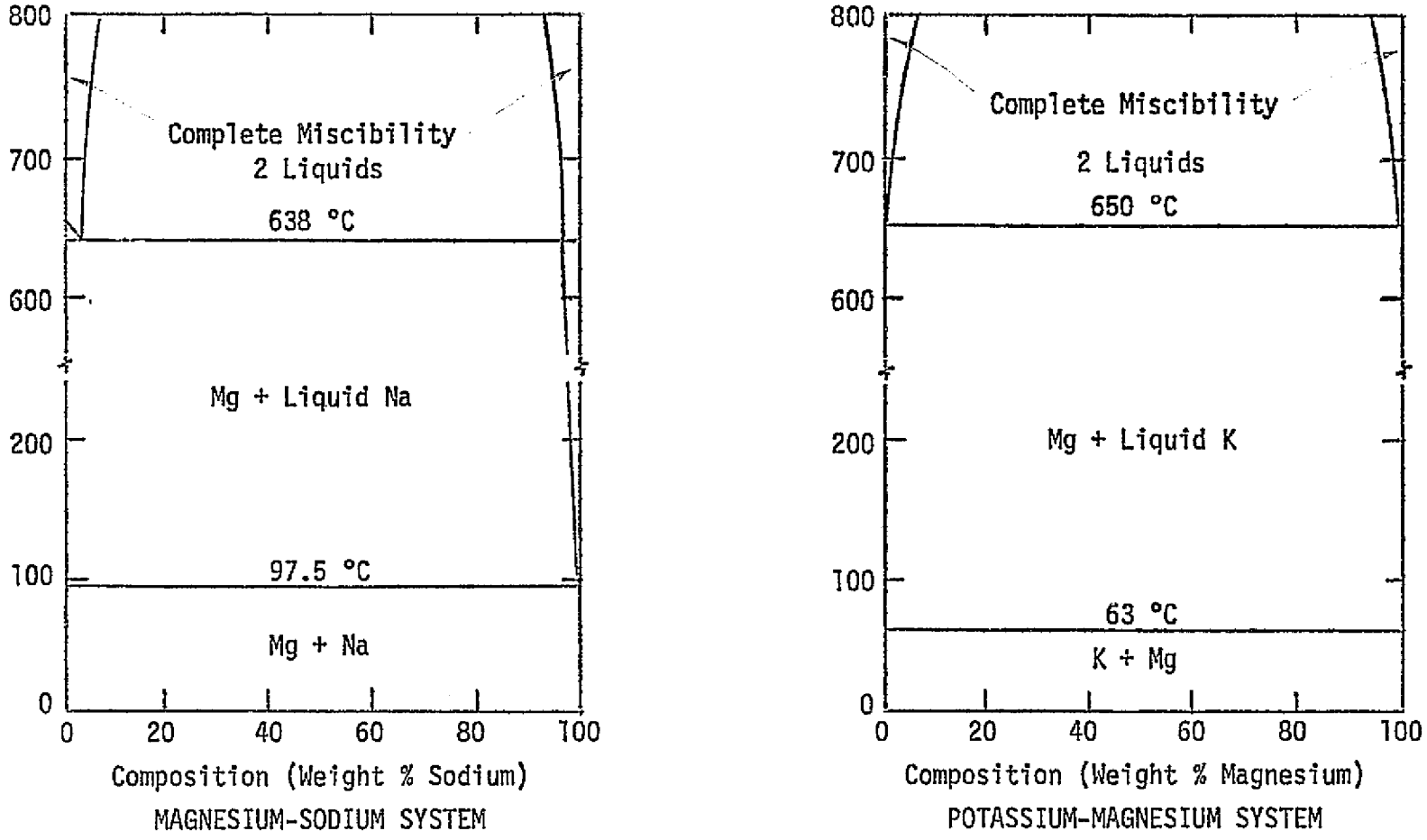

FIGURE 6 Phase Diagrams for the Magnesium-Sodium and Potassium Magnesium Systems.

battery power pack and timer unit. The test materials and materials used in the construction of the experimental package will be selected to be compatible with the temperature profile provided in the Space Shuttle Users Guide.

Special electrical, mechanical or control requirements are not required. The experiment will be initiated by a signal from an electrical timer module after release of the LDEF from the shuttle. The approximate temperature-time histories of the two categories of experiments are shown schematically in Figure 7. Upon final solidification the experiments will remain dormant until recovered. Setting of the timer to its sequence will be required prior to launch. It is anticipated here that installation of the experimental package on board LDEF and timer initiation will be undertaken by ground support crews.

The location of the experimental package on LDEF is not critical. Each sample module will be hermetically sealed and thermally insulated. However, it is desirable that there be a minimum of spacecraft attitude change during actual solidification of the test samples to avoid the possible generation of disturbances within the solidifying materials. The experiment will be attached to the experiment tray by means of a bolted joint employing reusable selflocking fasteners.

7.2 Environmental Conditions

The pre and post flight environment in the bay area of the Long Duration Exposure Facility will be controlled. A conditioned air purge will maintain the temperature in the range from 300K to 320K at a relative humidity of 50%. During flight the bay area is vented directly to the atmosphere.

During launch and reentry, the facility will be subjected to extremes in acoustic noise, vibration and gravitational loading. The variation of

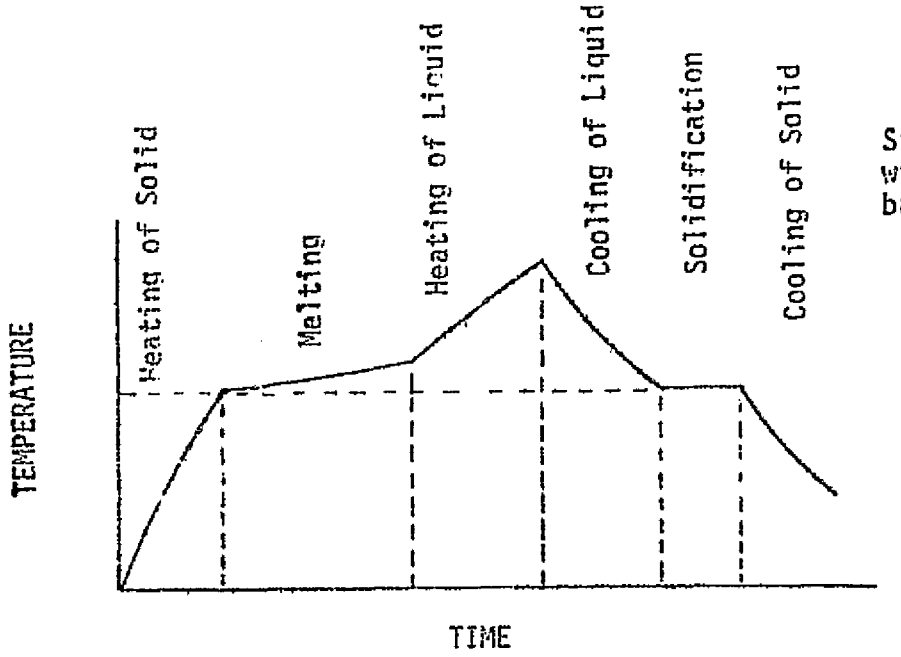

Six test capsules will follow same basic profile.

(i) Morphology Studies - Liquid stage temperature will depend on material selection.

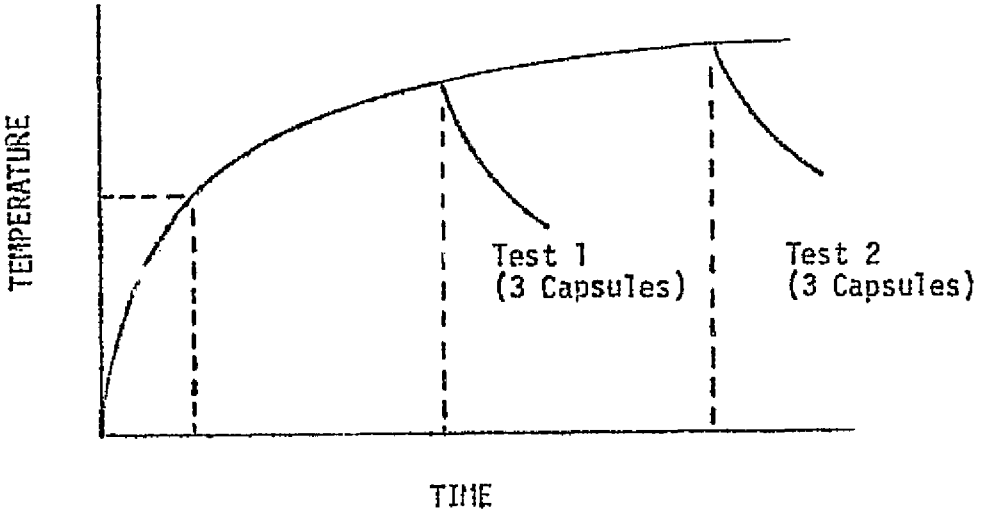

(ii) Convection Studies - Liquid stage temperature will depend on material selection.

FIGURE 7 Schematic Temperature - Time Profiles for Morphology and Convection Studies

these factors with time during the launch period are shown in Figures 8, 9 and 10. In flight it is anticipated that there will be an absence of external loads. However, a temperature variation throughout the facility is anticipated. The temperatures at various locations within the facility are given in Table IX. The temperature of space is assumed to be zero degrees absolute.

During reentry a sharp rise in temperature within the facility to 340K is anticipated. In addition the experimental package should be capable of withstanding a load equal to 20 times that due to normal gravity for a period of 11 milliseconds duration without suffering major damage. This should ensure that the package will remain intact should a major disaster occur (crash).

A shield provided by the National Aeronautics and Space Administration and installed prior to launch will nulify effects of radiation and partical bombardment during space exposure.

7.3 General Morphology Studies

7.3.1 Cell Description

The general concepts for the experiment concerned with a study of the general morphology and ullage space location for selected materials solidified in a ZERO-G environment have been developed in Section 5 of this report. The anticipated environmental and dynamic conditions have been described in the previous section. At the present time approximate analyses and calculations have been performed in order to generate a preliminary design for the experimental package. These analyses and calculations will be refined in the final design stage.

Figure 11 shows the preliminary configuration for the test cell proposed for the general morphology studies with important dimensions. The

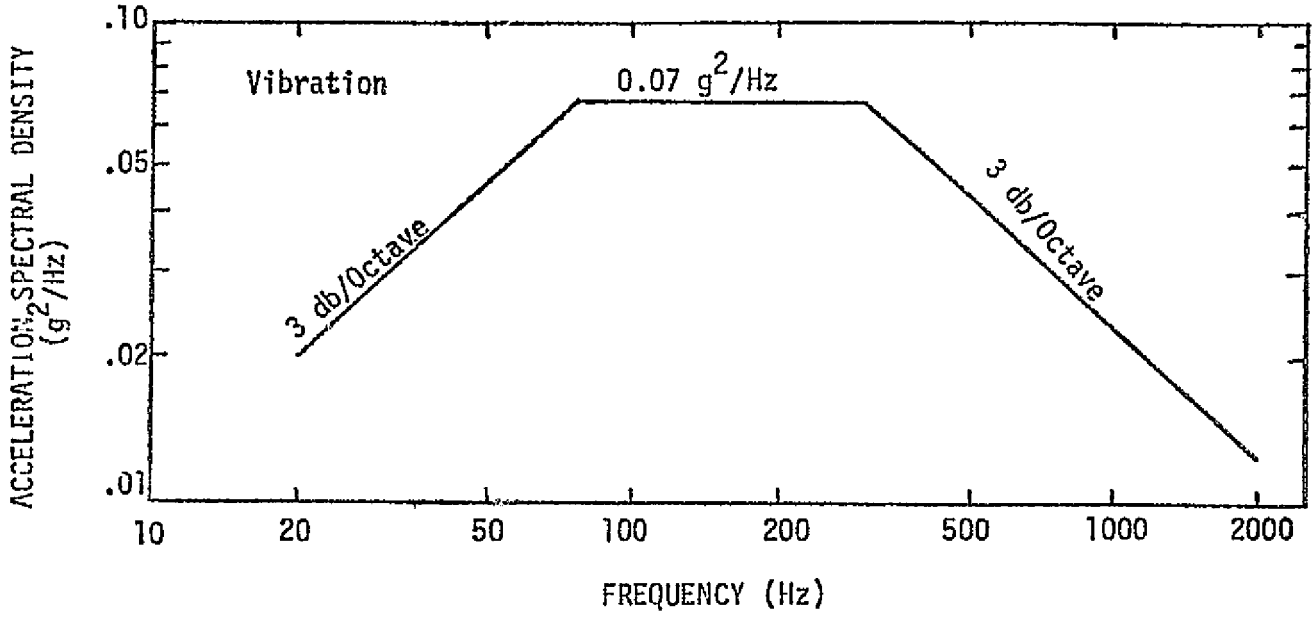

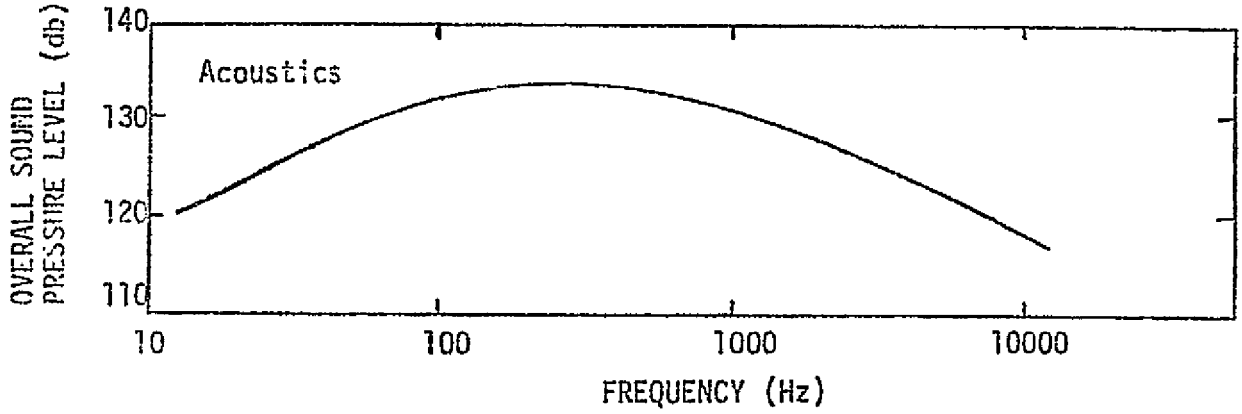

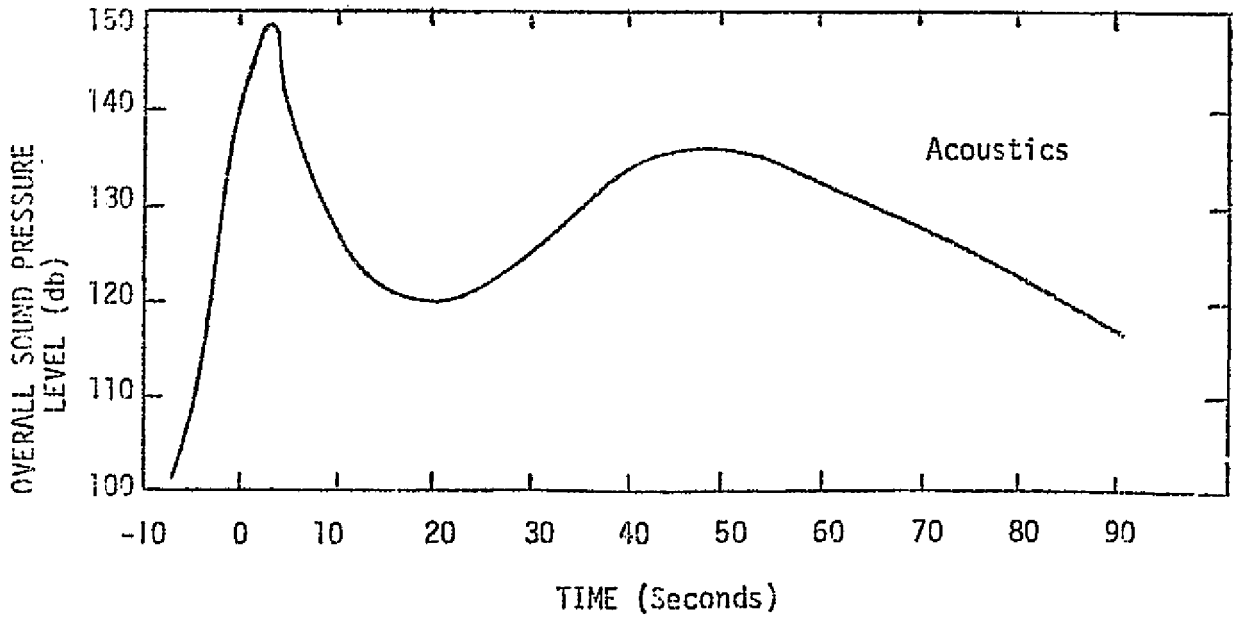

FIGURE 8 Launch Environment (Approximately 9 Minutes Duration)

Launch Environment

Maximum Acceleration, g

x: -3.3 y: ± 1.0 z: ± 1.5

Temperature:

Slow Steady Rise From

70°F to 80 °F

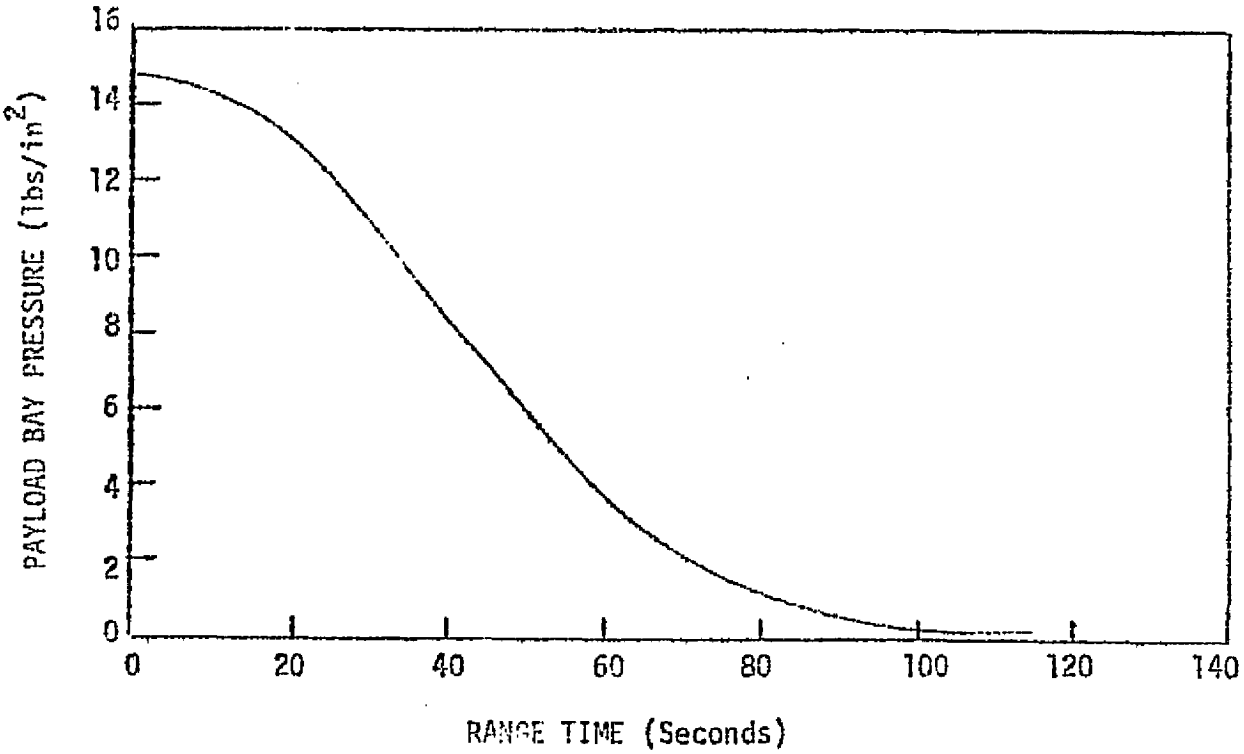

FIGURE 9 Launch Environment

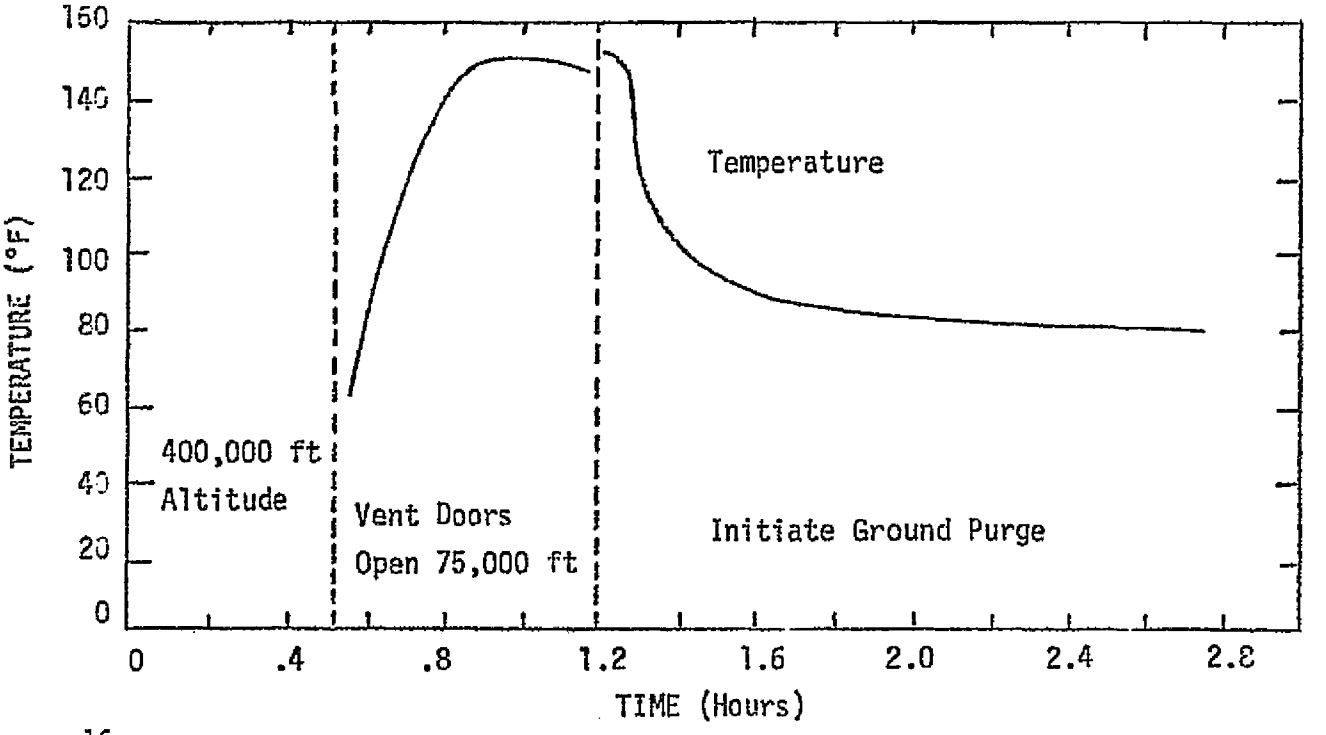

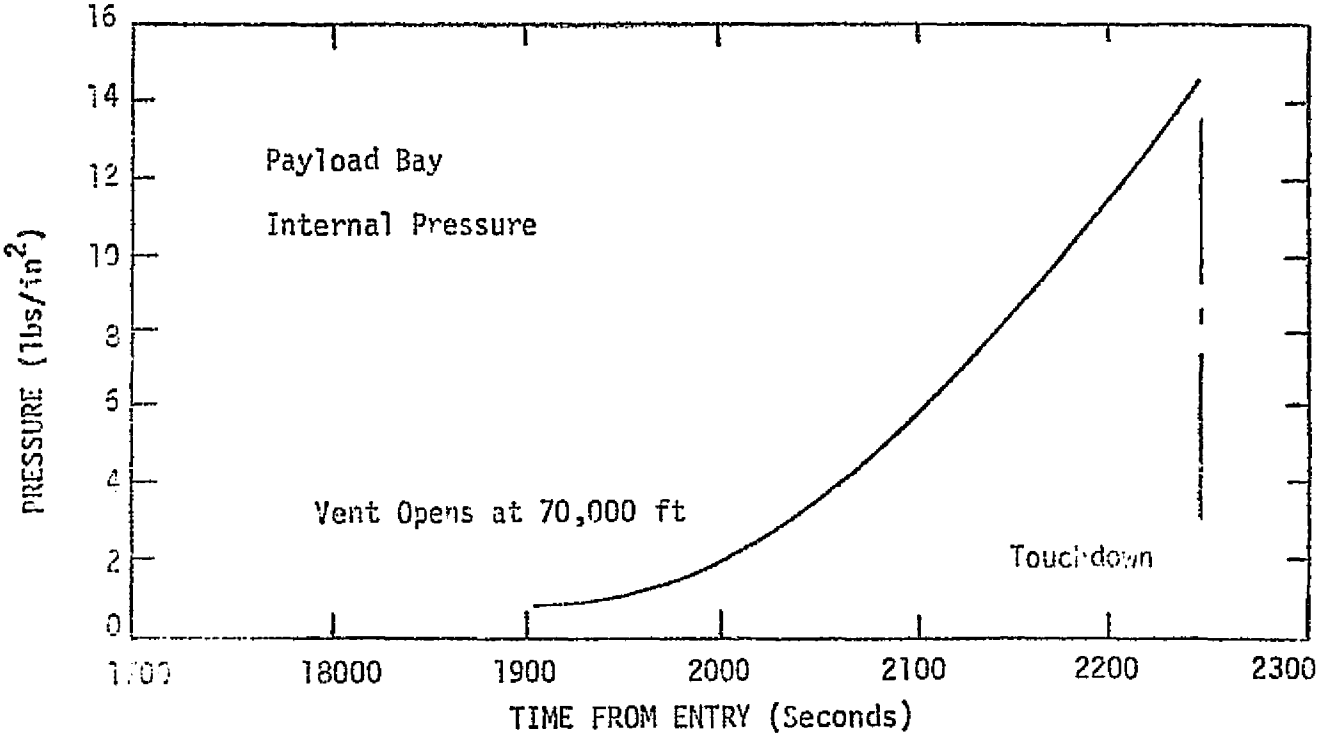

Maximum Accelerations, g: Vibration: Negligible

x: ± 1.06 y: ± 1.25 z: ± 2.8 Acoustics: Negligible

FIGURE 10 Entry Environment (Approximately 40 Minutes Duration).

TABLE IX Typical Temperature Ranges at Various Locations on Spacecraft for Orbital Environment

Location	Temperatures (°F)		
	Minimum	Maximum	Typical ΔT/Orbit
internal	-25	45	10-20
Earth end	9	75	30-60
Space end	-104	45	100-150
Experiment tray	-72	116	67
White paint	-110	31	67
Black paint (not exposed to sun)	-57	52	18

Additional conditions:

(i) Time in sunlight: 62% - 72% of orbit period, orbit period: 94.6 minutes

(ii) Time to steady state thermal cycle: approximately 10 orbits (16 hours)

(iii) Space environment: 0°Rankine

(iv) Orientation

Maximum "G" Level at release 2×10^{-6}G

Maximum "G" Level, steady-stale 1×10^{-6}G

X Axis is directed outward from earth

Z Axis is in direction of spacecraft velocity vector

cell has been made in such a way that it can be disassembled easily to retrieve the test material after both ground testing and actual space exposure. Each test cell consists of a heating unit (H) attached to a cylindrical sub base (B) and cylindrical body (C) with a common set of bolts. The rim of the heating unit is separated from the sub base and cell body with a layer of thermal insulating material. A separate diagram of the heating unit is shown in Figure 12. The cylindrical specimen (S) is press fitted into the cell body in such a way that it rests adjacent to the heating element (H) and cell liner (L). The sides of the heating element (H) are isolated from the cell with electrical and thermal insulation (I). With this arrangement it is hoped that conditions of unidirectional heat conduction with a change of phase can be established. The cell is sealed with a screw threaded cylindrical cap (P).

The completed cell is placed in a recess is a locating base (LB). Common bolts of the self-locking type are used to attach the completed cell and locating base to the experiment tray (T). The locating base will be made from rubber and will serve as a pad to dampen vibration of the test cell during launch and landing.

7.3.2 Stress Analysis

The direct loading to which the test cell is exposed is negligible. However, stresses may arise because of the increase in pressure of the encapsulated gasses, differential thermal expansion of the test cell and sample during the heating phase of the thermal cycle, and large volume changes associated with the change in phase (solid⇄liquid) of the test material. Calculation of the stresses arising from these sources involves the application of standard procedures. In the following some typical stress levels will be given based on the extreme ranges of experimental

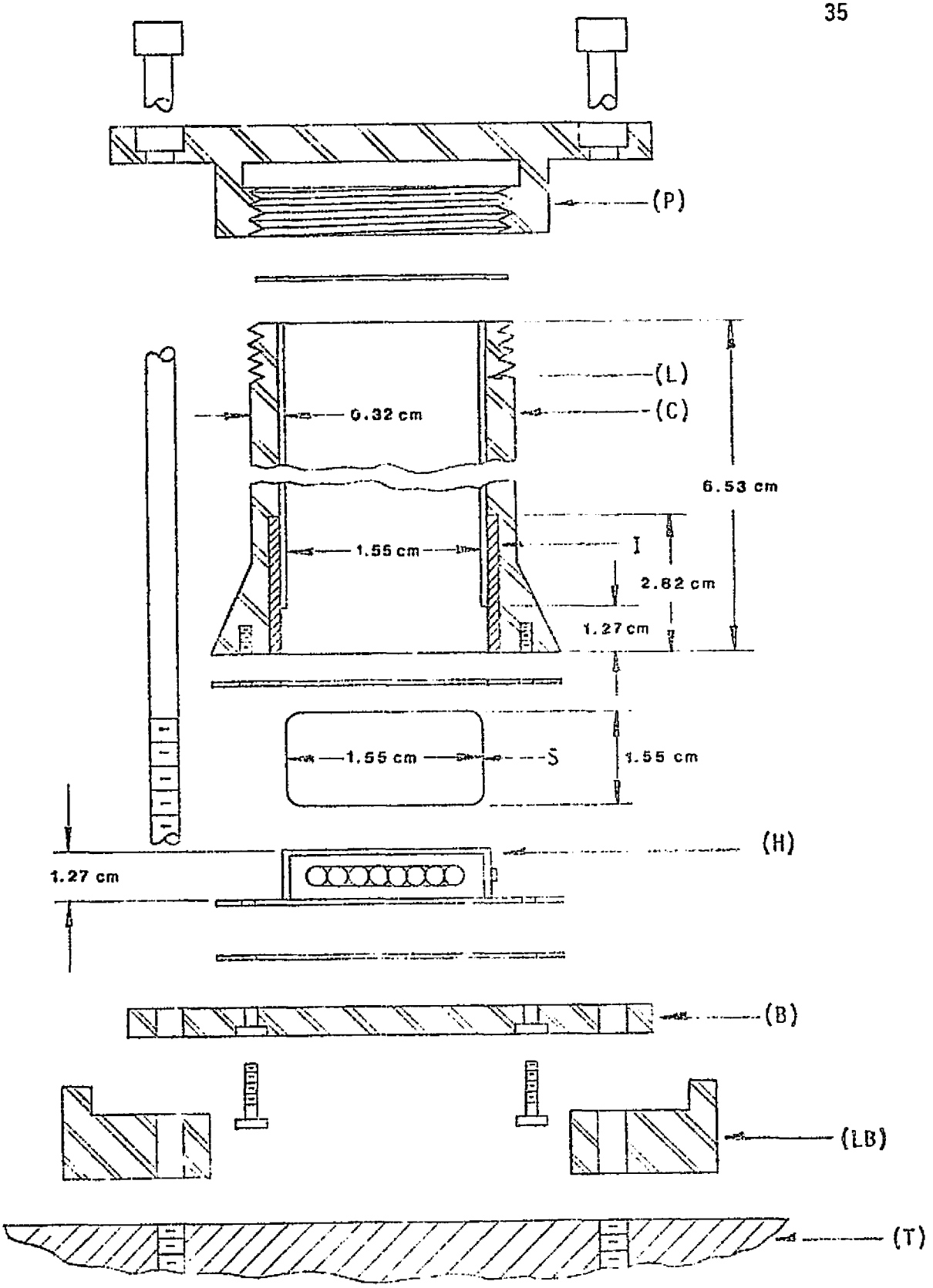

FIGURE 11 Test Cell For General Morphology Studies.

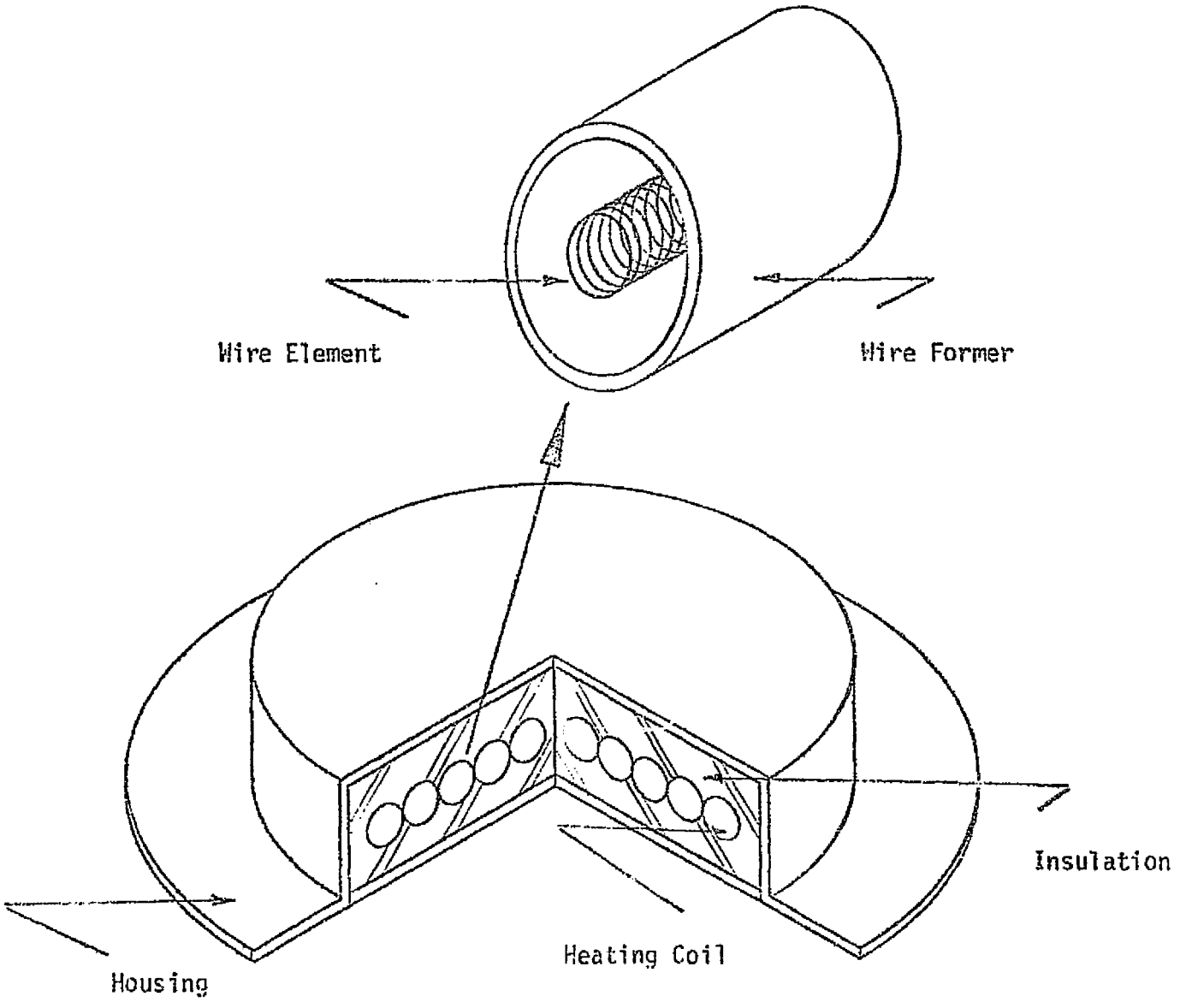

FIGURE 12 Schematic Diagram of Heating Unit.

conditions anticipated. Clearly, the actual stresses generated will depend upon the type of test material used. The computations are based on the dimensions given in Figure 11.

If it is assumed that the entrapped gas (argon) is initially at normal ambient temperature and pressure (298°K, 1.01×10^5 N/m^2) and is subjected to a temperature increase of 600°K then an internal pressure of 2.96×10^5 N/m^2 will be generated. In turn, this will produce tangential and axial stresses of 7.23×10^5 N/m^2 and 3.61×10^5 N/m^2, respectively. Clearly, these are extremely small stresses.

When the encapsulated test material is heated it expands. If the coefficient of expansion of the test material is greater than that of the test cell then "interference" will occur and radial contact and tangential stresses will be produced in the cell. If it now assumed that an aluminum test sample is used with a stainless steel container and that the increase in temperature is 635°K, then a contact stress of 27×10^7 N/m^2 will be produced. A temperature rise of 635°K is sufficient to heat the aluminum from ambient temperature to its melting point. The physical and mechanical properties used in the calculations were obtained from standard sources [13]. In turn, the radial contact stress will induce in the test cell a tangential stress of 76.0×10^7 N/m^2.

When the test material melts it undergoes an expansion of approximately 5%. In the early stages of melting the melted portion of the test material will tend to move the unmelted material along the test cell because of an increase in pressure within the liquid. If it is now assumed that the coefficient of friction between the cell and test sample is 0.4 and that a contact stress of 27×10^7 N/m^2 exists across the cell-test piece interface then melting will induce an axial stress of 43×10^7 N/m^2 in the base of the

cell walls. A coefficient of friction of 0.4 is the value found most often experimentally for sliding of metal pairs under dry, unlubricated conditions.

It can be seen from the above that substantial stresses can be generated by thermal expansion and melting of the test material. However, it is pointed out that compressive stresses will be applied directly to the test cells through the retaining bolts. These stresses will tend to be counteract those generated in the base of the cell because of expansion and melting of the test material. In the final design careful attention will be paid to the encapsulation procedures used and the generation thermal and contact stresses.

7.3.3 Thermal Analysis

For the present experiment it is necessary to determine the time taken and amount of heat required to raise the temperature of the test sample from a prescribed initial temperature to the melting point temperature, then to bring about complete melting.

The theoretical analysis described in the following applies to the case of uniaxial heat conduction with a change of phase. The entire analysis is divided into two parts which describe the complete heating history. The first part of the analysis (premelting regime) is concerned with heating of the test material from some initial temperature to the melting point temperature. The second part is concerned with the melting of the test sample (melting regime). The analysis is based on the integral heat balance approach first proposed by Goodman [15].

For the premelting and melting regimes the basic model on which the present analysis is based is shown in Figures 13 and 14. For the premelting regime the following initial assumptions are made:

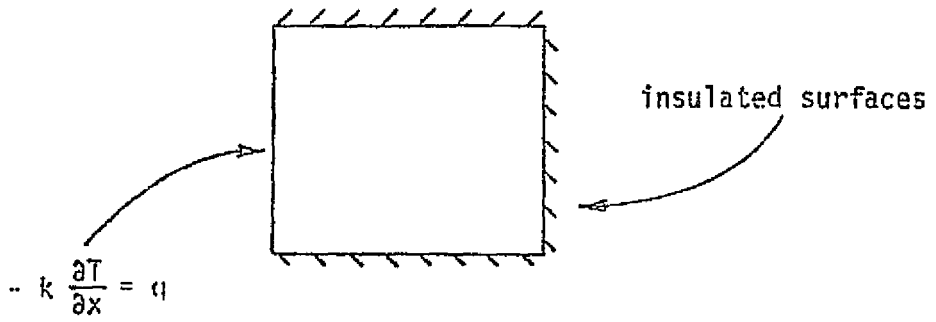

(i) boundary conditions

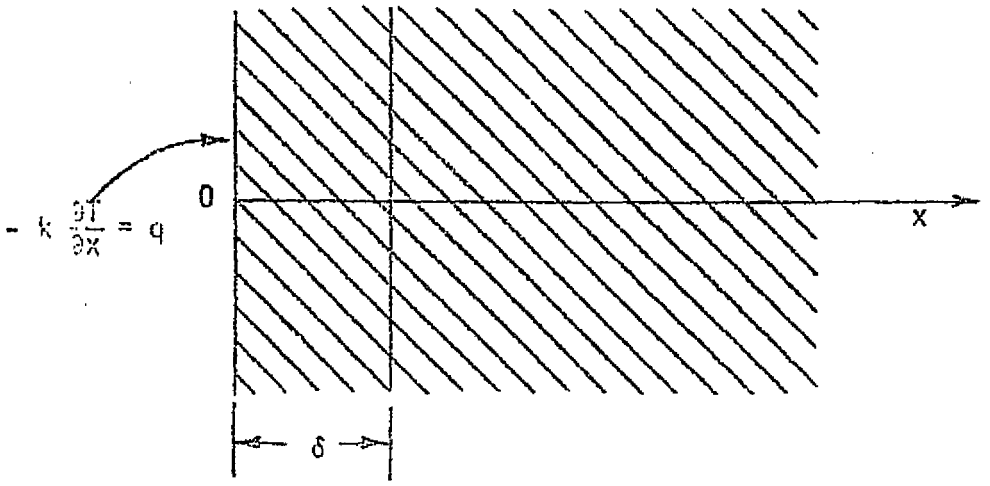

(ii) thermal boundary

FIGURE 12 Thermal Model For Premelting

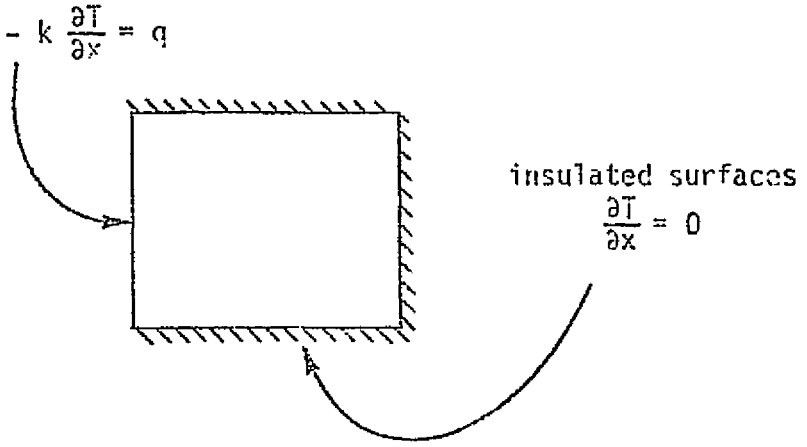

(i) boundary conditions

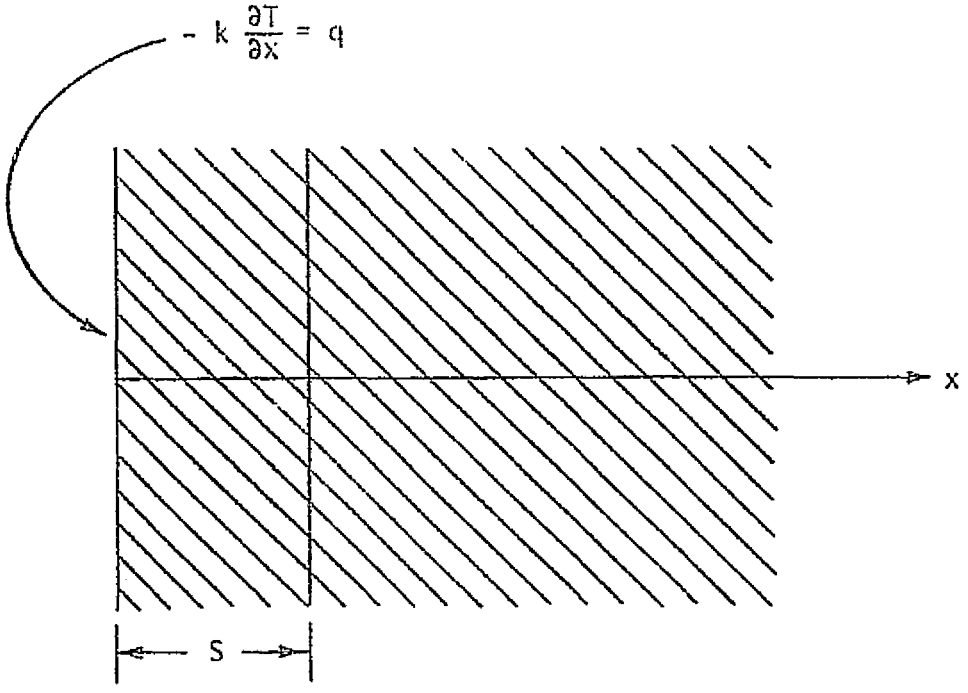

(ii) solid liquid interface

FIGURE 14 Thermal Model for Melting

(i) The test sample is at some initial uniform temperature below the melting point temperature; for simplicity the initial temperature is taken as zero.

(ii) A heat flux of magnitude q is applied at the boundary x = 0.

(iii) The problem is one of transient uniaxial heat conduction.

(iv) A thermal layer is assumed of thickness $\delta(t)$, $t > 0$.

(v) The boundary at x = L is insulated.

The aforementioned assumptions lead to the following differential equation:

$$\frac{\partial^2 T(x,t)}{\partial x^2} = \frac{1}{\alpha}\frac{\partial T(x,t)}{\partial t} \quad \text{in the region} \quad 0 \le x \le \delta \quad , \quad t > 0 \; . \tag{1}$$

The boundary conditions are:

$$\frac{\partial T(x,t)}{\partial x} = 0 \quad \text{at} \quad x = \delta \text{ (and } x = L) \quad , \quad t > 0 \tag{2}$$

$$q = -\frac{k\partial T(x,t)}{\partial x} \quad \text{at} \quad x = 0 \quad , \quad t > 0 \; . \tag{3}$$

The initial condition is:

$$T(x,t) = 0 \quad \text{in the region} \quad 0 \le x \le L \quad , \quad t = 0 \; . \tag{4}$$

The thermal boundary condition is:

$$T(x,t) = 0 \quad \text{at} \quad x = \delta(t) \quad , \quad t > 0 \; . \tag{5}$$

Using the approach developed by Goodman [15] it can be shown that the temperature distribution in the solid is given by:

$$T(x,t) = \frac{q}{k}\left\{\frac{\sqrt{6\alpha t}}{2} - x + \frac{x^2}{2\sqrt{6\alpha t}}\right\} \; . \tag{6}$$

When the thermal layer advances to the end of the test sample,

$$x = L \quad , \tag{7}$$

$$t = \frac{L^2}{6\alpha} \quad , \tag{8}$$

and

$$T(x, \frac{L^2}{6\alpha}) = \frac{qL}{2k} \quad , \quad x = 0 \ . \tag{9}$$

When the melting point temperature of the solid is greater than that given by equation (9), a second heating stage must be considered. Again, using the approach developed by Goodman [15] it can be shown that the temperature distribution is given now by:

$$T\left(x, t > \frac{L^2}{6\alpha}\right) = \frac{q}{kL}\left\{\frac{1}{3}(3\alpha t + L^2) - xL + \frac{1}{2}x^2\right\} \ . \tag{10}$$

Equation (10) is valid for:

$$\frac{L^2}{6\alpha} < t < t_m \ , \tag{11}$$

where t_m is the time required to begin melting. For a material which has a melting point T_m above the initial temperature, the time at which melting begins is given by:

$$t_{(melting)} = \frac{(3T_m kL - L^2 q)}{3\alpha q} \ . \tag{12}$$

Preliminary calculation has shown that for most materials considered for the present investigation the actual temperature gradient across the test sample is small at the beginning of melting. In order to simplify the problem for the melting regime, the following assumptions are made:

(i) The problem is one of uniaxial heat conduction with a change of phase.

(ii) The test sample is at some initial uniform temperature T_m, the melting point temperature. For simplicity the initial temperature is taken as zero.

(iii) A heat flux of magnitude q is applied at the boundary x = 0.

(iv) A melted layer is assumed of thickness s(t), t > 0.

The aforementioned assumptions lead to the following differential equation:

$$\frac{\partial^2 T(x,t)}{\partial x^2} = \frac{1}{\alpha}\frac{\partial T(x,t)}{\partial t} \quad \text{in the region} \quad 0 \le x \le L \quad , \quad t > 0 \; . \tag{13}$$

The boundary conditions are:

$$q = -\frac{k\partial T(x,t)}{\partial x} \quad \text{at} \quad x = 0 \quad , \quad t > 0 \; , \tag{14}$$

$$\frac{\partial T(x,t)}{\partial x} = 0 \quad \text{at} \quad x = L \quad , \quad t > 0 \; . \tag{15}$$

The initial condition is:

$$T(x,t) = 0 \quad \text{in the region} \quad 0 \le x \le L \quad , \quad t = 0 \; . \tag{16}$$

The solid-liquid interface thermal equilibrium condition is:

$$-\frac{k\partial T(x,t)}{\partial x} = \rho L_T \frac{d}{dt}\{s(t)\} \quad \text{at} \quad x = s \; . \tag{17}$$

It is assumed that the thermal properties of the liquid and solid phases are identical.

Using the approach developed by Goodman it can be shown that the position of the solid-liquid interface (s) and time (t) are related by the expression:

$$\tau = \frac{\bar{X}}{6}\{\bar{X} + 5 + (1 + 4\bar{X})^{1/2}\} \tag{18}$$

where,

$$\tau = \frac{q^2 t}{\alpha \rho^2 L_T^2} \; , \tag{19}$$

and

$$\bar{X} = \frac{qs}{\alpha \rho L_T} \; . \tag{20}$$

It can also be shown that the temperature distribution in the liquid phase is given by the expression:

$$T(x,t) = b(x - s) + c(x - s)^2 \tag{21}$$

where b and c are "constants" and are given by:

$$b = \frac{\alpha\rho L_T}{2ks(t)} \left[1 - \left\{ 1 + \frac{4qs(t)}{\alpha\rho L_T} \right\}^{1/2} \right] \tag{22}$$

and

$$c = \frac{k}{2\alpha\rho L_T} \left[\frac{\alpha\rho L_T}{2ks(t)} \left[1 - \left\{ 1 + \frac{4qs(t)}{L_T} \right\}^{1/2} \right] \right]^2 . \tag{23}$$

The temperature along the boundary at which the heat flux is applied is given by:

$$T(0,t) = \frac{\alpha\rho L_T}{k} \left\{ -\frac{1}{4} + \frac{1}{4} (1 + 4\bar{X})^{1/2} + \frac{\bar{X}}{2} \right\} . \tag{24}$$

Finally, equations (18) and (24) are shown graphically in Figures 15 and 16.

The equations given above can be used directly to determine the complete time-temperature histories for the heating and melting of test samples of any material for a given heat flux at the boundary. For the melting regime the location of the solid-liquid interface and temperature at the heat source (x = 0) for any time can be determined directly from Figures 15 and 16.

Attempts to analyse the solidification process have not been made because formulation of an appropriate model is not possible. It is anticipated that an appreciable amount of liquid migration will occur particularly in those situations where the liquid wets the contain walls making proposition of a model very difficult.

7,3.4 Application of Thermal Analysis

In order to demonstrate the application of the thermal analysis described in Section 7.3.3, the time required to melt a test sample of Bismuth

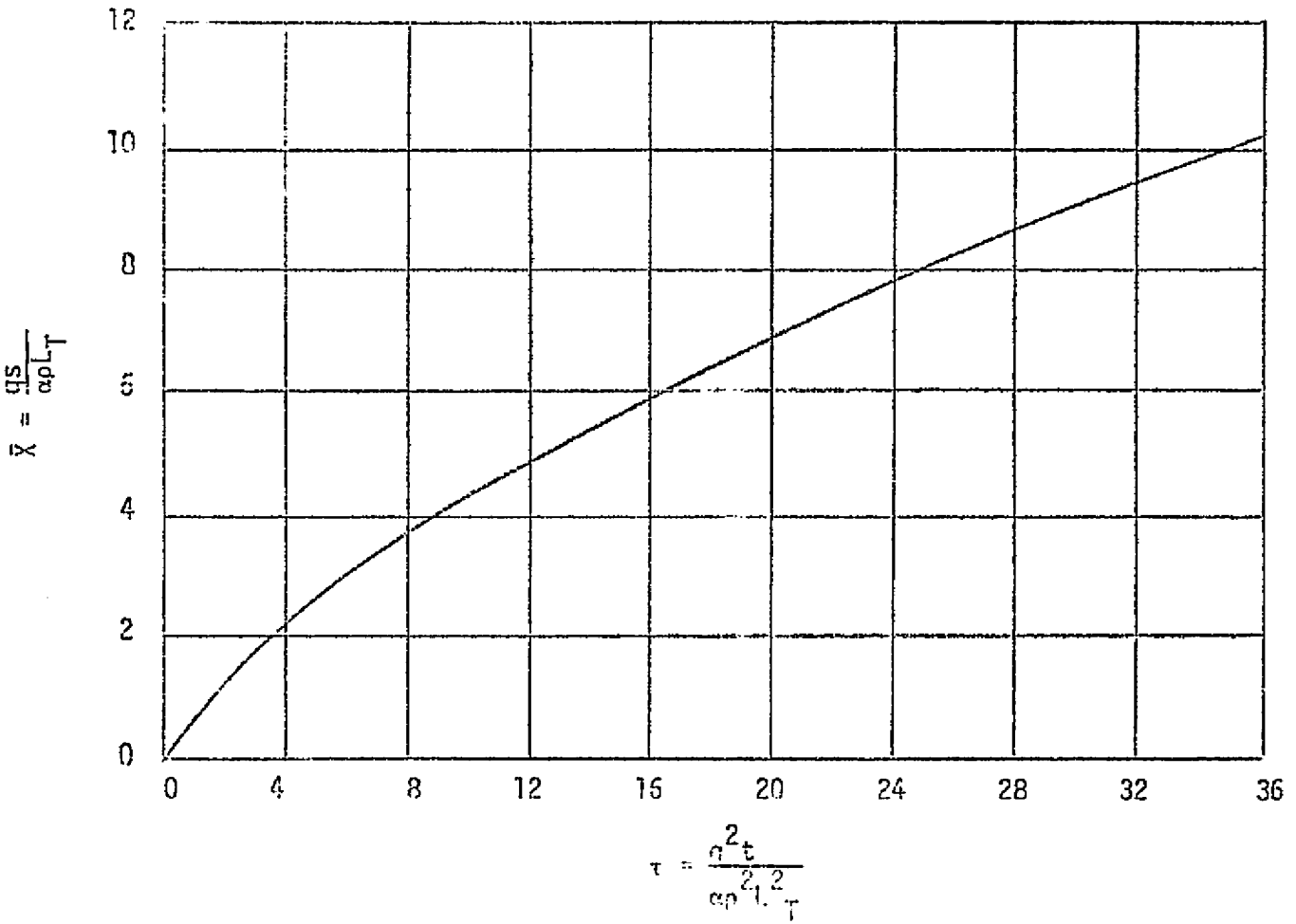

FIGURE 15 Variation of Thickness of Melted Region as a Function of Time.

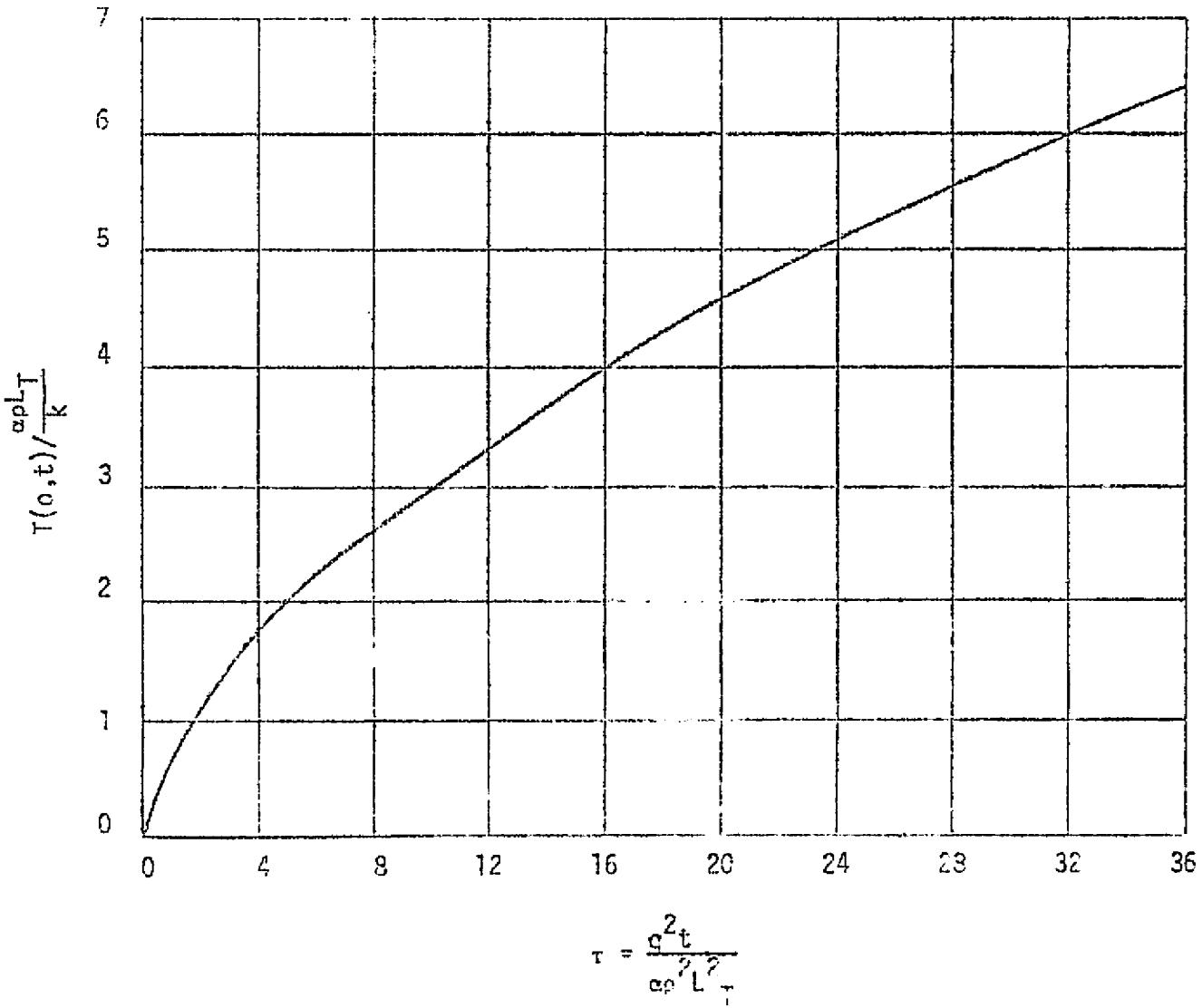

FIGURE 16 Temperature of Heat Source (x = o) as a Function of Time.

will be determined. It is believed that the predictions from the mathematical analysis and the experimental results to be generated from ground based preflight testing should establish beyond doubt the ability of the experimental package to perform the required functions.

The thermal properties of Bismuth are:

$$k = 0.084 \text{ watts/cm } ^\circ\text{C}$$

$$\rho = 9.8 \text{ gm/cm}^3$$

$$c_p = 0.029 \text{ cal/gm } ^\circ\text{C}$$

$$\alpha = 260 \text{ cm}^2\text{/hr}$$

$$L_T = 12.4 \text{ cal/gm}$$

$$T_m = 544.3^\circ\text{K}$$

The test sample is cylindrical with a height and diameter of 1.56 cm. The volume is 3.0 cm^3 and mass 29.4 gm.

In the present problem neither the heat flux nor the time required for complete melting are known. Therefore, an iterative procedure must be used to establish the appropriate values.

It is now assumed that a heat flux (q) of magnitude 1800 cal/cm^2 hr is applied to the test sample. The time required for the thermal boundary to traverse the length of the specimen is given by:

$$t_{traverse} = \frac{L^2}{6\alpha} \quad \text{(equation 8)} .$$

Substitution of the appropriate data gives:

$$t_{traverse} = 0.094 \text{ mins.}$$

The temperature distribution when the thermal boundary has traversed the specimen is given by:

$$T\left(x, \frac{L^2}{6\alpha}\right) = \frac{q}{k}\left\{\frac{L}{2} - x + \frac{x^2}{2L}\right\} \quad \text{(equation 10)} .$$

The temperature rise at the heat source (x = 0) is given by:

$$T\left(0, \frac{L^2}{6\alpha}\right) = \frac{qL}{2k}$$

$$= 19.4°C .$$

This temperature is below the melting point temperature for the test material and the second stage of the conductive heating phase must be considered. For:

$$t > \frac{L^2}{6\alpha}$$

the temperature distribution is given by:

$$T\left(x, t > \frac{L^2}{6\alpha}\right) = \frac{q}{kL}\left\{\frac{1}{3}(3\alpha t + L^2) - xL + \frac{1}{2}x^2\right\} \quad \text{(equation 10)} .$$

The time at which melting begins is given by:

$$t_{melting} = \frac{3T_m kL - L^2 q}{3q\alpha} + \frac{L^2}{6\alpha} \quad \text{(equation 12)} .$$

Substituting the appropriate data gives:

$$t_{melting} = 3.15 \text{ mins.} \quad \text{(a)}$$

The time to melt a given amount of test sample is given by:

$$\tau = \frac{\bar{X}}{6}\left[\bar{X} + 5(1 + 4\bar{X})^{1/2}\right] \quad \text{(equation (18)}$$

where

$$\tau = \frac{q^2 t}{\alpha \rho^2 L_T}$$

and

$$\bar{X} = \frac{qs}{\alpha \rho L_T} .$$

Substitution of the appropriate data and the condition s = L gives:

$$t_{\text{melting period}} = 6.61 \text{ min.} \quad \text{(b)}$$

The total time for heating and melting is the sum (a + b). Hence,

$$t_{TOTAL} = (3.15 + 6.61) \text{ min.}$$

$$t_{TOTAL} = 9.8 \text{ min.}$$

The temperature at the heat source (x = 0) when the sample is completely melted, is given by:

$$T(0, t_{TOTAL}) = \alpha\rho L_T\left[-\frac{1}{4} + \frac{1}{4}(1 + 4\bar{X})^{1/2} + \frac{\bar{X}}{2}\right]$$

$$T(0, 9.76) = 35°C \text{ (above melting point temperature)} .$$

In the above calculation ambient temperature has been taken as zero degrees centigrade.

A heat flux of 1800 cals/cm^2 hr corresponds to a total heat input of 576 cals and an assumed total melting time of 10 minutes. It is pointed out here that these values must be increased slightly to account for the fact that the analysis for the melting regime assumes the solid is at a uniform temperature equal to its melting point temperature and that some conductive heat losses will occur. When melting begins a temperature distribution will exist in the solid phase. The additional heat required to elevate the temperature of the solid uniformly to its melting point can be computed easily. Estimates of these heat losses will be made from experiments.

7.4 General Convection Studies

7.4.1 Convection in a ZERO-G Environment

When liquids solidify the predicted rates of solidification based on a conduction model of the freezing process and experimentally measured values often differ considerably. This difference is usually attributed to

convection. Convection may be driven by forces associated with buoyancy, surface tension, volume changes, external loading and electric or magnetic fields. The most important forces are those associated with buoyancy and surface tension. In a normal ONE-G environment buoyancy driven convection usually predominates whereas in a ZERO-G environment it is to be expected that surface tension driven convection would predominate.

The so-called Bond Number may be used to obtain a measure of the relative magnitudes of buoyancy and surface tension driven convection. The Bond Number is given by:

$$B_o = \frac{\rho g L^2}{\sigma} \quad . \tag{25}$$

For a Bond Number less than unity ($B_o < 1$) surface tension driven convection predominates whereas for a Bond Number greater than unity ($B_o > 1$) buoyancy driven convection predominates. Figure 17 shows the relative dominance of buoyancy and surface tension driven convection as a function of the characteristic length and dimensionless gravity. A measure of the magnitude of buoyancy driven convection can be obtained from the so-called Rayleigh Number. The Rayleigh Number is given by:

$$R_a = \frac{g \beta L^3}{\nu \alpha} (T_s - T_m) \quad . \tag{26}$$

In a space environment the Rayleigh Number becomes vanishingly small.

Surface tension driven convection is called often Marangoni Flow after the Italian scientist who first discovered the effect. Surface tension driven convection can occur when a temperature gradient exists along a phase boundary. The effect is greatest when steep temperature gradients exist along a liquid-gas interface. The effect arises because temperature gradients along a phase interface induce variations in surface tension and hence,

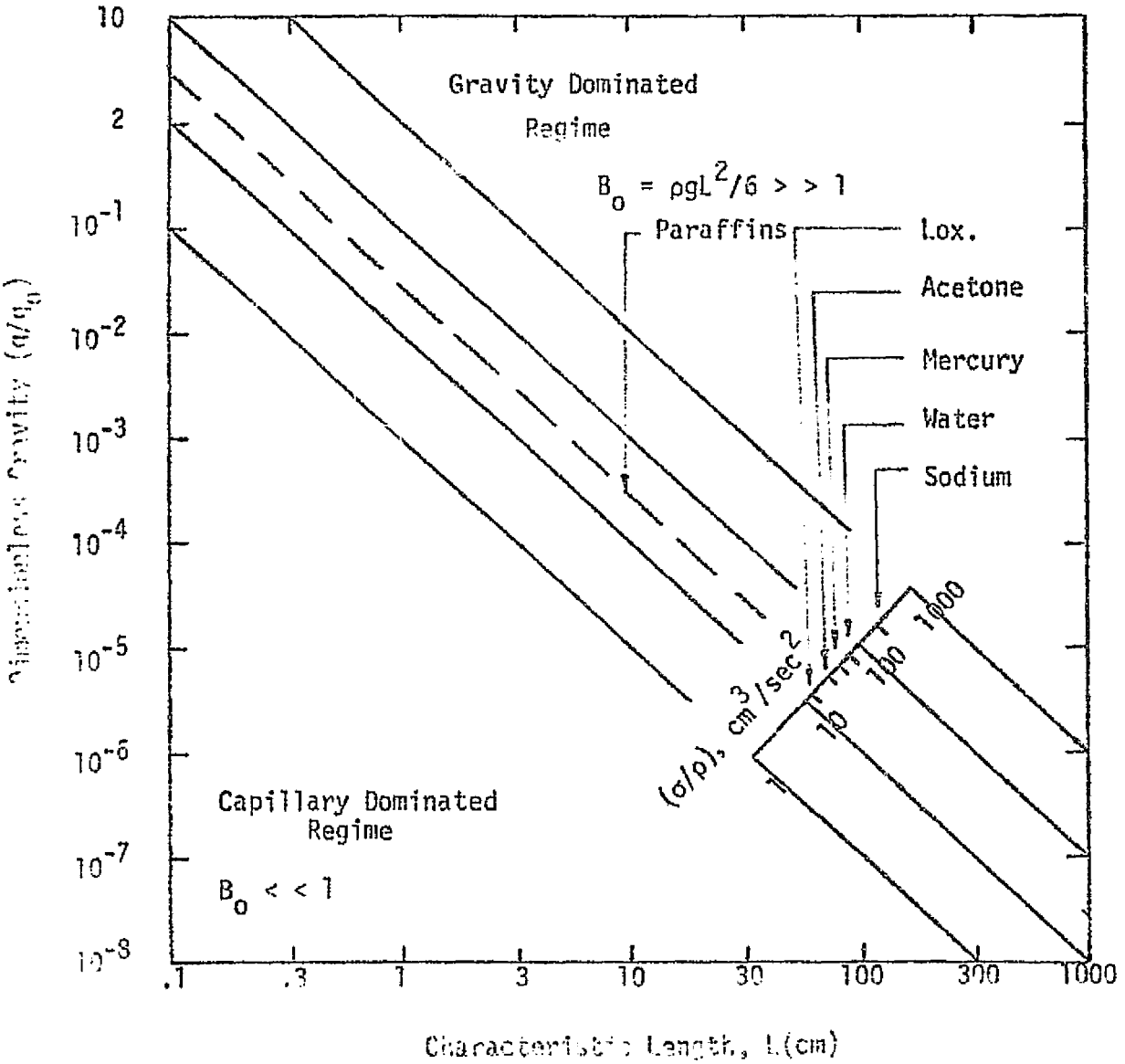

FIGURE 17 Hydrostatic Regimes for Typical Liquids

the magnitude of the interfacial stresses. In turn, the variation in shear stresses from point to point along an interface induce fluid flow and hence, convection. Surface tension is usually linearly dependent upon temperature according to the expression:

$$\sigma = \sigma_o - bT \ . \tag{27}$$

It can be seen that an increase in temperature produces a decrease in surface tension. The result is that fluid flow takes place from regions of high temperature to regions of lower temperature. The general characteristic of Marangoni Flow is shown in Figure 18.

The so-called Marangoni Number may be taken as a measure of the magnitude of surface tension driven convection. The Marangoni Number is given by:

$$M_a = \frac{\text{Surface Tension Forces}}{\text{Viscous Forces}}$$

or

$$M_a = - \frac{\left(\frac{d\sigma}{dt}\right)\left(\frac{dT}{dL}\right) L^2}{\rho \nu \alpha} \ . \tag{28}$$

The critical Marangoni Number for a fluid fixed between a rigid and free surface is 80.

7.4.2 Cell Description

The general concepts for the experiment concerned with a study of surface tension driven convection in a ZERO-G environment have been developed in Section 5 of this report. The anticipated environmental and dynamic conditions have been described in Section 7.2. At the present time approximate analyses and calculations have been performed in order to generate a preliminary design for the experimental package. These analyses will be refined in the final design stage.

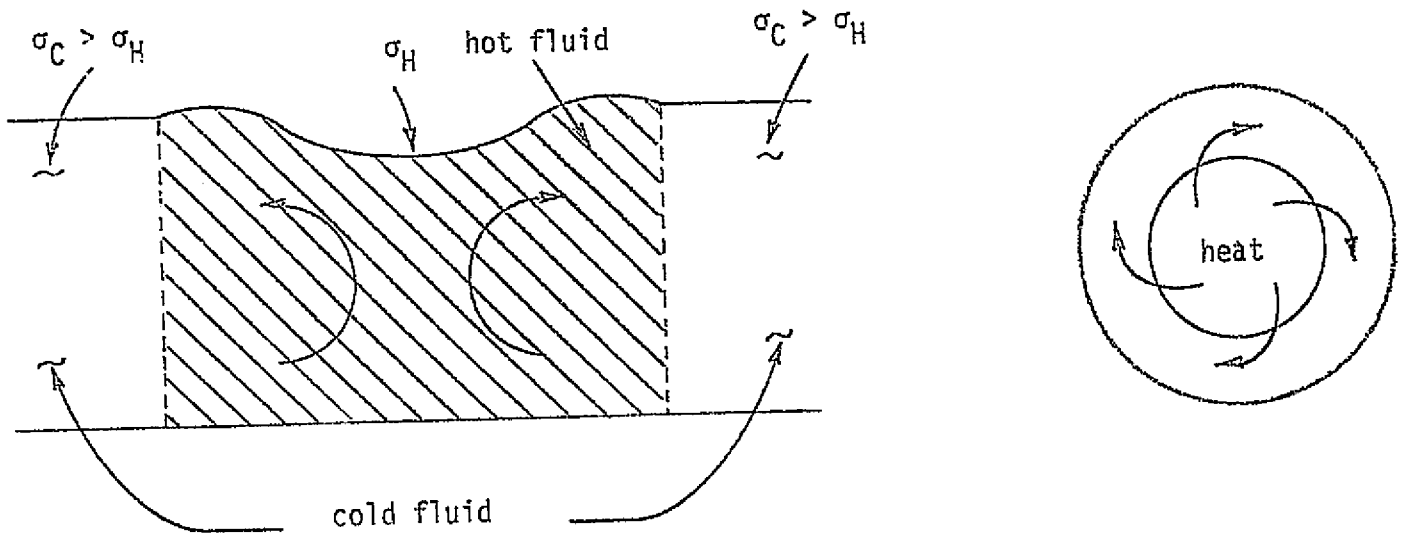

FIGURE 10 Surface Tension Driven Convection

Figure 19 shows the preliminary configuration for the test cell for the studies of surface tension driven convection. The cell has been made in such a way that it can be disassembled easily to retrieve the test material after both ground testing and actual space exposure.

The specimen (S) is hemispherical in shape and rests in a recess in a base (B). The specimen (S) is separated from the base (B) by a thin layer of thermal and electrical insulating material (I). A heater (H) and heat shields (HS) are placed above the specimen and rest in a shoulder in the base (B). The lower heat shield (HS) has a small orifice at the center in order to generate a heat source on the flat circular face of the test specimen. The test cell is sealed with a screw threaded cylindrical cap (P). The completed cell is placed in a recess in a locating base (LB). Common bolts of the self-locking type are used to attach the completed cell and locating base to the experiment tray (T). The locating base will be made from rubber and will serve as a pad to dampen vibration of the test cell during launch and landing.

With the aforementioned arrangement it is believed that conditions of uniaxial (in radial direction) heat conduction with a change of phase can be generated. Complete melting of the test specimen will not be carried out. Melting will be continued only to the point where pools of melted material of predetermined size are established.

7.4.3 Stress Analysis

The direct loading to which the test cell is exposed is negligible. In addition, the stresses generated because of an increase in temperature of the encapsulated gases, differential expansion of test cell and sample during the heating phase of the thermal cycle and large volume changes associated

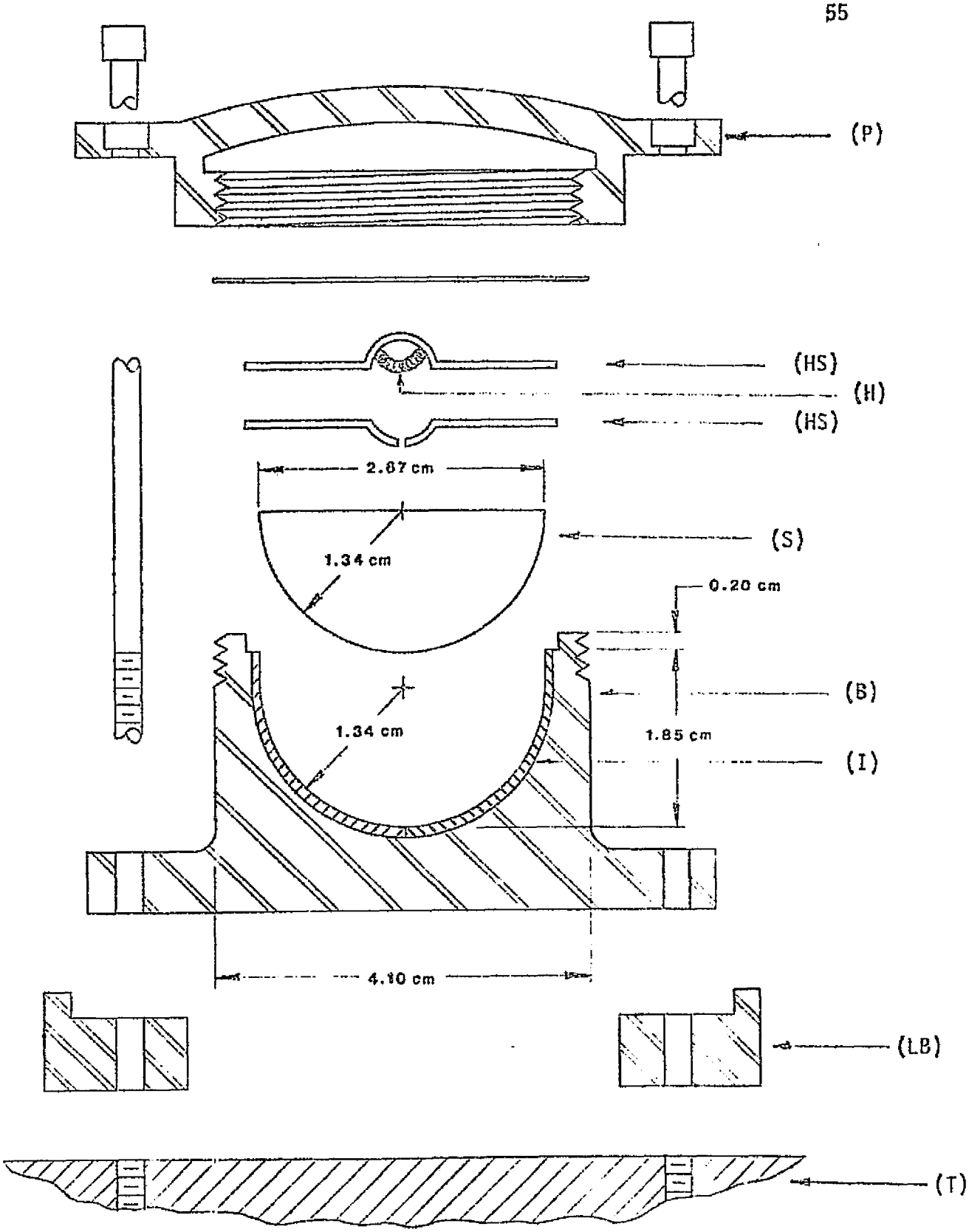

FIGURE 19 Test Cell for Convection Studies

with the change in phase (solid⇄liquid) of the test sample also are negligible. Hence, a rigorous mechanical analysis is not required.

7.4.4 Thermal Analysis

For the present experiment it is necessary to determine the time taken and amount of heat required to heat the test sample and produce a predetermined degree of melting.

The theoretical analysis described in the following applies to the case of uniaxial heat conduction with a change of phase. The entire analysis is divided into two parts which describe the complete heating history. The first part of the analysis (premelting regime) is concerned with heating of a portion of the test material from some initial temperature to the melting point temperature. The second part (melting regime) is concerned with the partial melting of the test sample to generate a molten pool supported by unmelted material. The analysis is based on the integral heat balance approach first proposed by Goodman [15].

For the premelting and melting regimes the basic model on which the present analysis is based is shown in Figures 20 and 21. For the premelting regime the following initial assumptions are made:

(i) The test sample is at some initial uniform temperature below the melting point temperature; for simplicity the initial temperature is taken as zero.

(ii) A heat flux of magnitude q is applied over the area enclosed by the conic $r = a$.

(iii) The problem is one of uniaxial heat conduction.

(iv) A thermal layer is assumed of thickness $\delta(t)$, $t > 0$.

(v) The boundary at $r = b$ is insulated.

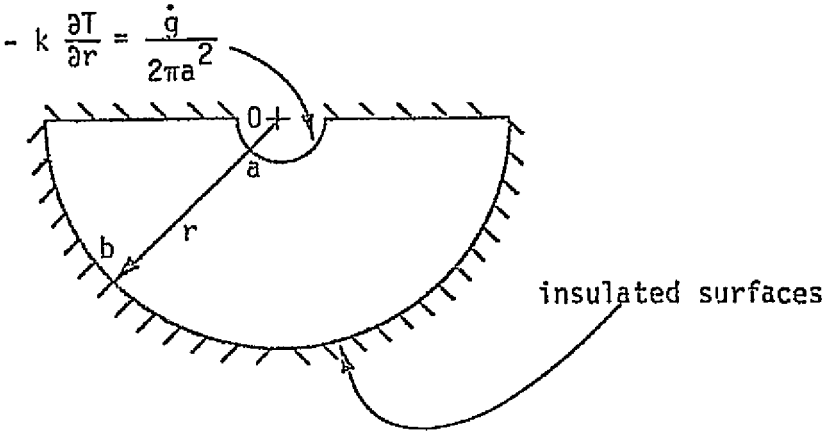

(i) boundary conditions

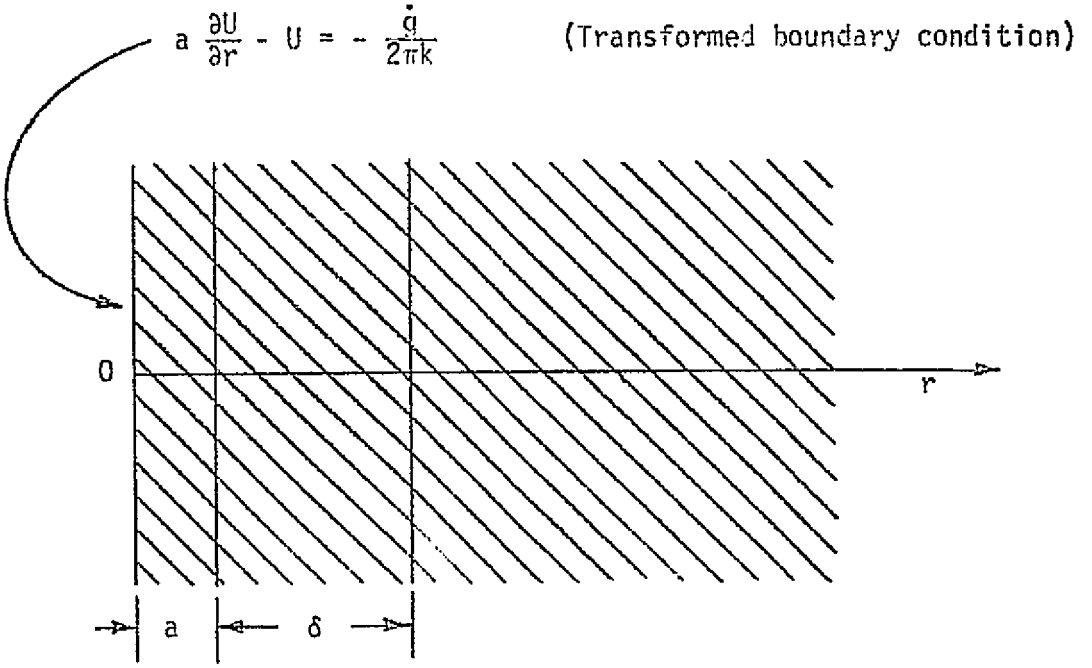

(ii) thermal boundary

FIGURE 20 Thermal Model for Premelting Regime

$$-k \frac{\partial T}{\partial r} = \frac{\dot{q}}{2\pi a^2}$$

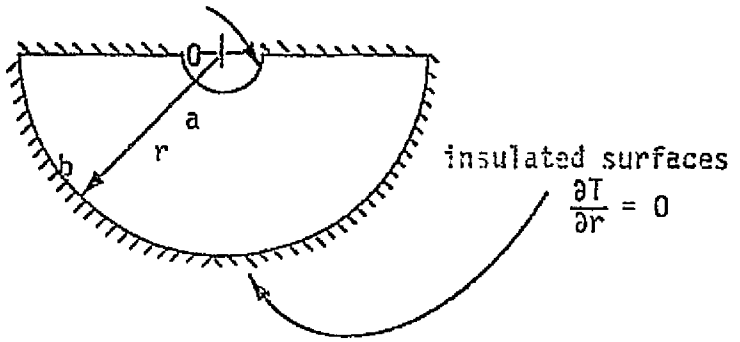

(i) boundary conditions

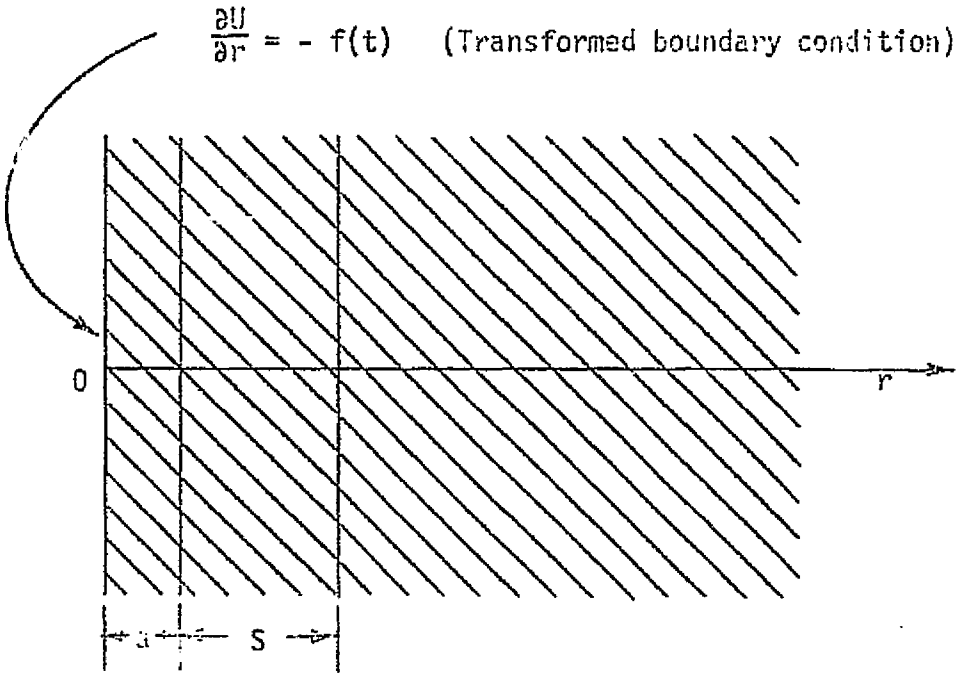

(ii) solid liquid interface

FIGURE 21 Thermal Model for Melting Regime

The model of the process described above leads to the following differential equation:

$$\frac{1}{r}\frac{\partial^2(r\cdot T(r,t))}{\partial r^2} = \frac{1}{\alpha}\frac{\partial T(r,t)}{\partial t} \quad \text{in the region} \quad a \le r \le \delta(t) \quad , \quad t > 0 \; . \tag{29}$$

The boundary conditions are:

$$q = -\,k\,\frac{\partial T}{\partial r} \quad \text{at} \quad r = a \quad , \quad t > 0 \tag{30}$$

where

$$q = \frac{\dot{g}}{2\pi a^2}$$

$$\frac{\partial T}{\partial r} = 0 \quad \text{at} \quad r = \delta \quad (\text{and } r = b) \quad , \quad t > 0 \; . \tag{31}$$

The initial condition is:

$$T(r,t) = 0 \quad \text{in the region} \quad a \le r \le b \quad , \quad t = 0 \; . \tag{32}$$

The thermal boundary condition is:

$$T(r,t) = 0 \quad \text{at} \quad r = \delta(t) \quad , \quad t > 0 \; . \tag{33}$$

A new dependent variable $U(r,t)$ is defined by:

$$U(r,t) = (r)T(r,t) \; . \tag{34}$$

The differential equation now becomes:

$$\frac{\partial^2 U(r,t)}{\partial r^2} = \frac{1}{\alpha}\frac{\partial U(r,t)}{\partial t} \quad \text{in the region} \quad a \le r \le \delta(t) \quad , \quad t > 0 \; . \tag{35}$$

The boundary conditions become:

$$\frac{a\partial U(r,t)}{\partial t} - U(r,t) = -\,\frac{\dot{g}}{2\pi k} \quad \text{at} \quad r = a \quad , \quad t > 0 \tag{36}$$

$$\frac{\partial U(r,t)}{\partial r} = \frac{U(r,t)}{b} \quad \text{at} \quad r = b \quad , \quad t > 0 \tag{37}$$

$$\frac{\partial U(r,t)}{\partial r} = 0 \quad \text{at} \quad r = \delta(t) \quad , \quad t > 0 \tag{38}$$

$$U(r,t) = 0 \quad \text{at} \quad r = \delta(t) \quad , \quad t > 0 \; . \tag{39}$$

The initial condition becomes:

$$U(r,t) = 0 \quad \text{in the region} \quad a \leq r \leq b \quad , \quad t = 0 \; . \tag{40}$$

Using the integral heat balance approach developed by Goodman [15] it can be shown that the temperature distribution in the solid and location of the thermal boundary are given by:

$$T(r,t) = \frac{\dot{g}}{2\pi k r} + \frac{\dot{g}}{2\pi k(2a + \delta)\delta} \left\{\frac{a^2}{r} - 2(a + \delta) + r\right\} \tag{41}$$

and

$$t = \frac{1}{12\alpha} \left\{\delta^2 + 6a\delta - 8a^2 \log_e \left[\frac{\delta + 3a}{3a}\right]\right\} \tag{42}$$

respectively. The time taken (t) for the thermal layer to reach the boundary can be found by substituting:

$$\delta = (b - a) \tag{43}$$

into equation (42). The temperature at the heat source is then given by:

$$T(a,t_t) = \frac{\dot{g}}{2\pi k a} \left\{1 - \frac{2ab}{2ab + b^2}\right\} \; . \tag{44}$$

When the melting point temperature of the solid is greater than that given by equation (44) a second heating stage must be considered. Again, using the approach developed by Goodman [15] it can be shown that the temperature distribution is given now by:

$$T(r,t > t_t) = -\frac{\dot{g}(r - a)}{2\pi k a r} + \frac{\dot{g}(b - a)}{2\pi k(a + b)} \cdot \left[\frac{1}{a} + \frac{(r - a)^2}{(b - a)^2 r}\right] e^{K_o(t - t_t)} \; . \tag{45}$$

Equation (45) is valid for:

$$t_t < t < t_m$$

where t_m is the time required to begin melting. For a material which has a melting point T_m above the initial temperature the time at which melting occurs is given by:

$$t_{melting} = \frac{1}{K_o} \log_e \left\{\frac{a T_m^2 \pi k(a + b)}{\dot{g}(b - a)}\right\} + t_t \tag{46}$$

where

$$K_o = \frac{12a\alpha}{8a(b-a)^2 - 3(b-a)^3} . \tag{47}$$

Preliminary calculation has shown that for most materials considered for the present investigation, the actual temperature gradient across the test sample is small at the beginning of melting. In order to simplify the problem for the melting regime, the following assumptions are made:

(i) The problem is one of uniaxial heat conduction with a change of phase.

(ii) The test sample is at some initial uniform temperature T_m the melting point temperature. For simplicity the initial temperature is taken as zero.

(iii) A heat flux of magnitude q is applied over the area enclosed by the conic r = a.

(iv) A melted layer is assumed of thickness s(t), t > 0.

The aforementioned assumptions lead to the following differential equation.

$$\frac{\partial^2 U(r,t)}{\partial r^2} = \frac{1}{\alpha}\frac{\partial U(r,t)}{\partial t} \quad \text{in the region} \quad a < r < s(t) \quad , \quad t > 0 . \tag{48}$$

The boundary conditions are:

$$\frac{a\partial U(r,t)}{\partial r} - U(r,t) = -\frac{\dot{q}}{2\pi k} \quad \text{at} \quad r = a \quad , \quad t > 0 \tag{49}$$

$$\frac{\partial U(r,t)}{\partial r} = 0 \quad \text{at} \quad r = b \quad , \quad t > 0 . \tag{50}$$

The initial condition is:

$$U(r,t) = 0 \quad \text{in the region} \quad a \leq r \leq b \quad , \quad t = 0 . \tag{51}$$

The solid-liquid interface thermal equilibrium condition is:

$$\frac{\partial U(r,t)}{\partial r} = -\frac{\rho L_T}{k} s(t) \frac{ds(t)}{dt} \quad \text{at} \quad r = \delta + a \quad , \quad t > 0 . \tag{52}$$

It is assumed that the thermal properties of the liquid and solid phases are identical.

A rigorous solution to the melting problem posed above is difficult and beyond the scope of the preliminary design phase of the present project. However, an approximate solution may be obtained easily if it is assumed that:

$$\frac{\partial U}{\partial r} = - f(t) \quad \text{at} \quad r = a \quad , \quad t > 0 \tag{53}$$

and that the function f(t) is related to the heat flux by the expression:

$$- f(t) = \frac{q}{a} (1 - e^{-w/t}) \tag{54}$$

where w is a constant. This implies that the temperature at the heat source boundary (r = a) will continue to rise until the heat flux becomes vanishingly small.

Using the aforementioned simplification and the approach developed by Goodman, it can be shown that the position of the solid-liquid interface can be obtained from the expressions:

$$\int_0^t f(t')dt' = \frac{\rho L_T s^2}{6k} \{\bar{\mu} + (1 + 4\bar{\mu})^{1/2} + 2\} \tag{55}$$

where

$$\bar{\mu} = \frac{f(t)k}{\rho L_T \alpha} \quad . \tag{56}$$

The relationship between $\bar{\mu}$ and $\frac{6k}{\rho L_T s^2} \int_0^t f(t')dt'$, a factor involving the location of the solid-liquid interface is shown in Figure 22.

It can also be shown that the temperature distribution and temperature at the source surface as a function of time are given by the expressions:

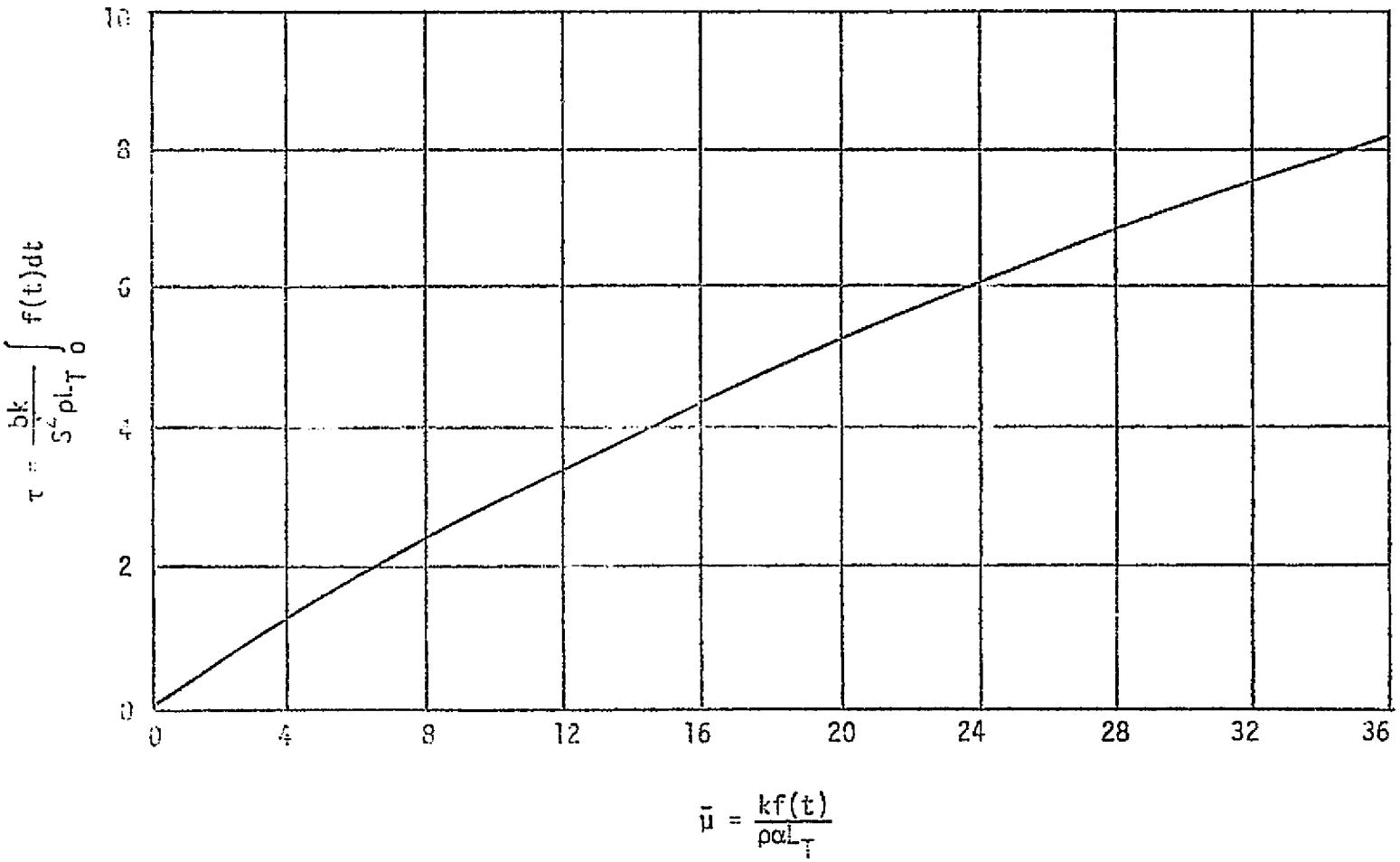

FIGURE 22 Variation of Thickness of Melted Region as a Function of Time.

$$U(r,t) = \frac{\rho L_T \alpha}{2k} \{1 - (1 + 4\bar{\mu})^{1/2}\} (r - a - s) +$$

$$\frac{\rho L_T \alpha}{4ks} \{[1 - (1 + 4\bar{\mu})^{1/2}] + 2\bar{\mu}\} (r - a - s)^2 \qquad (57)$$

and

$$U(a,t) = \frac{g e^{-w/t}}{2\pi k a} \qquad (58)$$

respectively.

The equations given above can be used directly to determine the complete time-temperature histories for the heating and melting of test samples of any material for a given heat flux at the boundary.

Attempts to analyse the solidification process have not been made because formulation of an appropriate model is not possible.

7.4.5 Application of Thermal Analysis

In order to demonstrate the application of the thermal analysis described in Section 7.4.4 the time required to melt a given amount of a test sample of the paraffin hydrocarbon Triacontane will be determined. It is believed that predictions from the mathematical analysis and the experimental results to be generated from ground based preflight testing should establish beyond doubt the ability of the experimental package to perform the required functions.

The thermal properties of Triacontane are:

L_T = 251 J/g^{4}n k = 0.149 J/δ m °K

ρ = 810 kg/m^3 α = 8.45 x 10^{-8} m^2/s

Cp = 2176 J/kg °K T_m = 359°K

$$\sigma = 33 \text{ dynes/cm}$$

$$v = 0.0073 \text{ N} \cdot \text{s/m}^2 .$$

The test sample is hemispherical in shape with a radius of 1.7 cm and a volume of 10 cm^3. The radius of the heat flux is 0.127 cm.

In the present problem neither the heat flux nor the time required for melting a given volume (or mass) of material are known. Therefore, an iterative procedure must be used to establish appropriate values.

It is now assumed that a heat rate ($\dot{g}$) of magnitude 554.4 cal/hr is applied to the test sample. The time required for the thermal boundary to traverse the sample to the insulated layer is given by:

$$t = \frac{1}{12\alpha}\left\{\delta^2 + 6a\delta - 8a^2 \log_e\left[\frac{\delta + 3a}{3a}\right]\right\} \quad \text{(equation 42)} .$$

Substitution of the appropriate data gives:

$$t_{traverse} = 5.0 \text{ mins.}$$

The temperature distribution when the thermal boundary has traversed the specimen is given by:

$$T(r,t_{traverse}) = \frac{\dot{g}}{2\pi kr} + \frac{\dot{g}}{2\pi kr}\left[\frac{a^2 - 2(a + \delta)r + r^2}{\delta(2a + \delta)}\right] \quad \text{(equation 41)} .$$

The temperature rise at the heat source (r = a) is given by:

$$T(a,t_{traverse}) = \frac{\dot{g}}{2\pi ka}\left[1 - \frac{2ab}{(2ab + b^2)}\right] \quad \text{(equation 44)}$$

$$= 448°C .$$

It can be seen clearly that the temperature rise at the source is far in excess of the melting point temperature for Triacontane. Thus, melting begins before the thermal boundary has reached the outer boundary of the cell.

It is now necessary to determine the value of (δ) when the temperature at the heat source reaches the melting point temperature of the

material. Substituting the value for the melting point temperature into equation (41) gives:

$$\delta = 0.256 \text{ cm} .$$

Substituting this value for δ into equation (42) gives:

$$t = 18 \text{ s} \quad (a) .$$

This is the time for source boundary to reach melting point temperature of the material. Thus, the intermediate heating stage is not required for the present example.

Substitution of equations (54) and (56) into equation (55) and integrating gives:

$$\frac{6\dot{g}}{2\pi\rho L_T}\left\{t - \frac{t^2}{w}e^{-w/t}\right\} = s^2\left\{\frac{\dot{g}(1 - e^{-w/t})}{2\pi a\rho L_T\alpha} + \left[1 + \frac{4\dot{g}(1 - e^{-w/t})}{2\pi a\rho L_T\alpha}\right]^{1/2} + 2\right\} .$$

An iterative procedure is now used to solve the above equation for the constant (w), which was found to be:

$$w = 1.158 \text{ hr.}$$

The time required for melting a given volume of material where the location of the solid-liquid interface is specified can now be obtained readily by substituting the appropriate values for w and s into the above equation and solving for t. Substituting the above calculated value for w and arbitrarily selected solid-liquid interface position of s = 1.2 cm into the above equation gives:

$$t = 10 \text{ min} \quad (b) .$$

The total time to produce melting to a location defined by s = 1.2 cm is the sum (a + b). Hence,

$$t_{TOTAL} = (18 \text{ s} + 10 \text{ min})$$

$$t_{TOTAL} = 10.28 \text{ min.}$$

Further calculation shows that the temperature at the heat source (r = a) is 106°C above the melting point temperature. Calculation shows also that the Marangoni Number (Ma) is 1.24×10^5. Hence, pronounced surface tension effects should occur.

7.5 Power Supply

Selection of an appropriate power supply is one of the most critical aspects of the present experimental program. Failure of the power supply would prematurely terminate the experiments and prevent the collection of useful data.

The nature of the Long Duration Exposure Facility demands that the power supply be completely self contained. Consequently, it must be of the battery type. A number of battery manufacturers have been contacted and a literature survey made to determine the most appropriate battery system for the present application. The results of these efforts are summarized in this section of the report.

The general requirements for the power supply are: (i) must be capable of driving timer module, (ii) must be capable of providing sufficient power for heating test cells, (iii) must be sufficiently robust to withstand environmental conditions, (iv) must have a small initial current drain, (v) must have a long shelf life and (vi) must not pose any hazard. A number of candidate power supply systems are available including, Dry Batteries (Carbon-Zinc, Mercury-Silver Oxide), Wet Batteries (Lead-Acid, Nickel-Iron), and High Energy Batteries (Silver-Zinc, Silver-Cadmium). Of these the Carbon-Zinc, Nickel-Cadmium and Silver-Zinc are the most promising. Some general characteristics for these systems are given in Table X. It is believed that the Carbon-Zinc battery system is inferior to

TABLE X. Some Characteristics of Most Promising Power Supply Systems

Type of System	Operating Voltage	General Characteristics
Carbon-Zinc	1.5 volts/cell	Low cost, made in a variety of shapes and sizes, can operate over a wide range of discharge conditions, deteriorates rapidly at temperatures greater than 325°K.
Nickel-Cadmium	1.2 volts/cell	Excellent charge retention, good mechanical strength, indefinite storage life, wide range of operating temperature.
Silver-Zinc	1.5 volts/cell	High energy density, wide range of operating temperature and pressures, good mechanical strength.

the Nickel-Cadmium and Silver-Zinc systems because of poor thermal stability. Figure 23 shows a comparison of the energy densities on a volumetric and mass basis for the Nickel-Cadmium and Silver-Zinc systems. It can be seen clearly that the Silver-Zinc system has the greatest energy density.

Silver-Zinc batteries have been used previously in both manned and unmanned space missions and have excellent performance records. In the present work power requirements for various combinations of candidate tests materials have been computed using the analytical procedures developed above. It was found that six cells connected in series (9 volts, 22.5 watt-hrs) would provide sufficient power for the most adverse conditions with 25% of total capacity remaining after completion of experiments.

The total battery weight would be approximately 0.33 Kg with a volume of approximately 241 μm^3. The total cost would be approximately $300.00. It is proposed to place the battery pack in a hermetically sealed container.

7.6 Experimental Arrangement

A schematic arrangement of the experiment is shown in Figure 24. The battery power supply will consist of six Silver-Zinc cells connected in series to provide a potential of 9 volts and power of 22.5 watt-hrs. This will be sufficient to drive the timer modules and heating units. The timer modules have not been designed at this time. However, it is believed that a straight forward engineering effort is required and major problems are not anticipated.

It is proposed that the primary timer be set by the ground crew prior to launch. It will be set so as to actuate the secondary timers when the Long Duration Exposure Facility has reached a stable orbit. The units designated

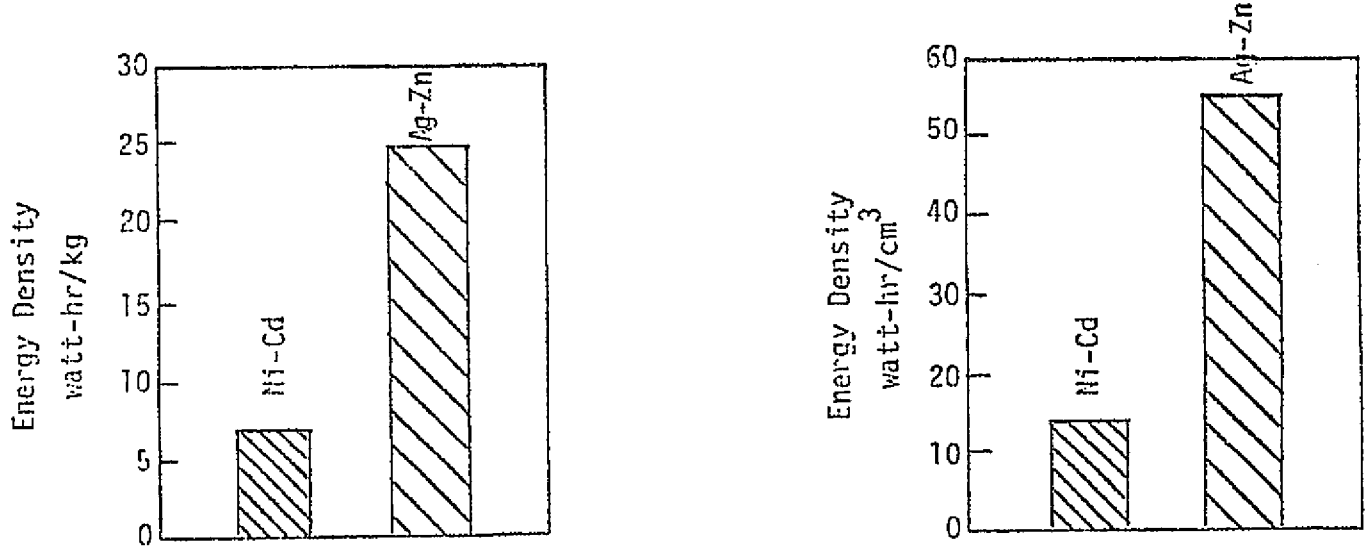

FIGURE 23 Relative Energy Densities of Nickel-Cadmium and Silver-Zinc Batteries

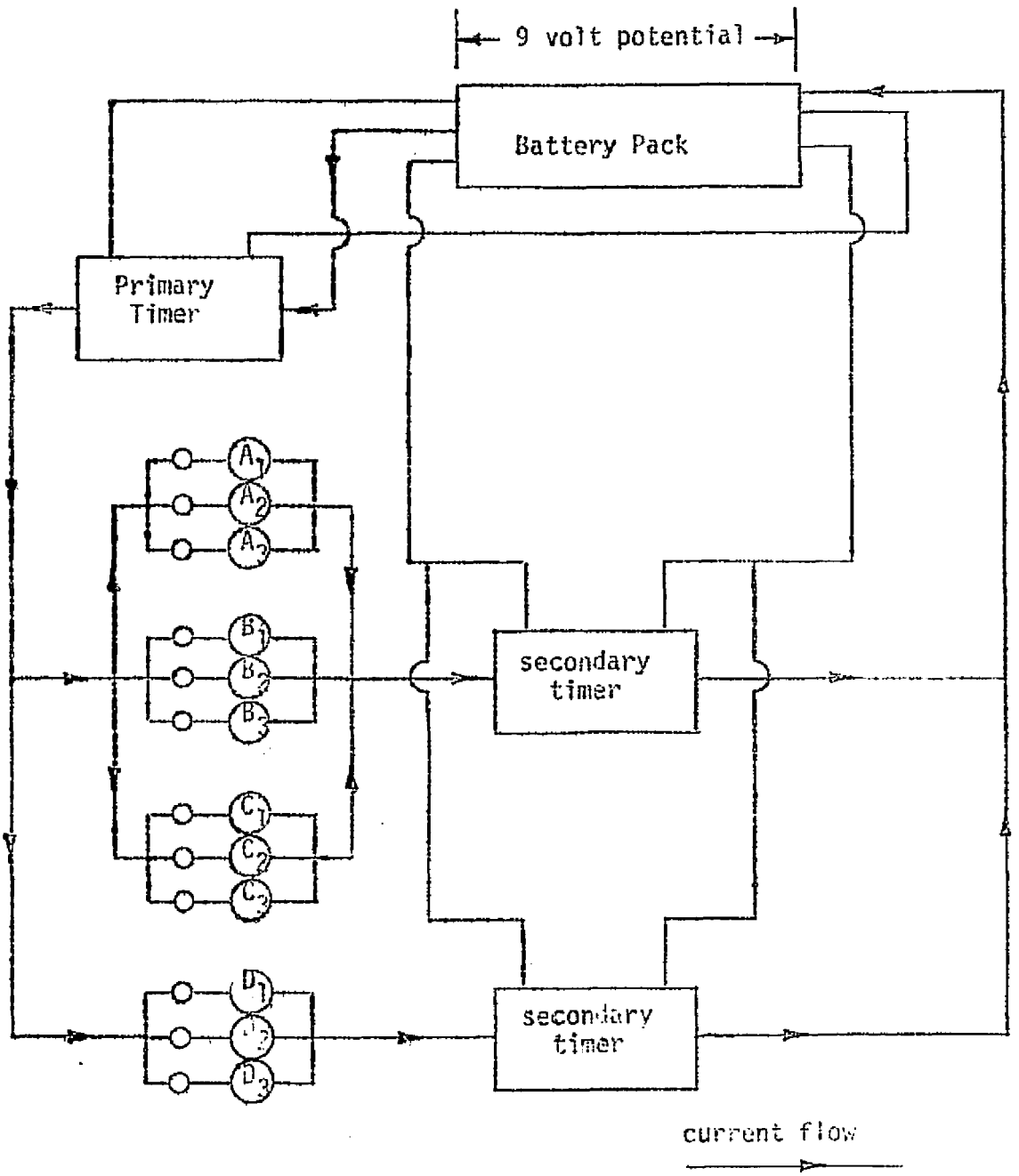

FIGURE 24 Schematic Diagram of Electrical System

A_1, A_2, A_3 and B_1, B_2, B_3 contain samples for the investigation of wetting conditions (wetting-nonwetting) on the general morphology of material solidified in a ZERO-G environment. The units designated C_1, C_2, C_3 and D_1, D_2, D_3 contain samples to investigate the phenomena of surface tension driven convection. Samples C_1, C_2 and C_3 will be heated for approximately 10 minutes; whereas samples D_1, D_2, and D_3 will be heated for approximately 30 minutes. After testing the experimental package will remain dormant until recovery.

In order to simplify the overall design of the experimental package temperature control will not be used. However, each test cell will be fitted with a fusible link so that should an electrical malfunction develop (short circuit) then the increase in current flow will cause the fusible link to melt and prevent excessive battery drain.

8. DATA REDUCTION AND ANALYSIS

Convection currents in fluids are usually driven by gravity in a ONE-G environment. However, gravity is not the only force capable of inducing fluid flow. Surface tension, interfacial tension, and volume changed associated with phase transformations (solid$\rightleftarrows$liquid) can serve as driving forces for fluid flow under the appropriate conditions.

Fluid flow caused by surface tension gradients is called Marangoni flow. If a liquid surface (liquid-vapor interface) is subjected to a temperature gradient then a surface tension gradient will be induced because surface tension is a function of temperature. Liquid will flow along the surface from regions of low surface tension (hot region) to regions of high surface tension (cold region). The velocity of fluid flow decreases with increasing depth beneath the surface: the depth of the disturbed region

depending upon many hydrodynamic factors. Concentration gradients can induce surface tension driven convection because surface tension is also a function of chemical composition.

In a ZERO-G environment gravity driven convection will be absent and surface tension driven convection should predominate. The present experiments have been devised to demonstrate the importance of surface tension in such an environment. The requirements of simplicity have precluded the generation of "on board" quantitative data. Data will be gathered by post flight analysis of tested samples.

Although the proposed experiments have been divided up into two categories they are in fact closely related. For both series of experiments the solidified test samples will be subjected to extensive post flight analysis. The analysis will consist essentially of sample characterization using a wide range of diagnostic techniques. The cylinders or cells containing the test samples will be examined first by X-Ray radiograpy then sectioned to expose the solidified surfaces. The surfaces will be examined using optical and scanning electron microscopy to determine both the macroscopic and microscopic geometry and characteristics of the surface. Next, the overall general shape of the solidified materials will be obtained by additional sectioning along planes parallel and perpendicular to the test cell axis. The sections will be prepared in the ususal way and examined in detail using optical microscopy to characterize thoroughly the general crystallography of the microstructure. Factors such as grain size, grain shape and grain orientation will be determined quantitatively. The samples will be examined also for the presence of general porosity, microporosity, and cracks. If detected their appearance, size, and distribution will be determined quantitatively by standard procedures. Selected areas of the

specimens will be examined using X-Ray diffraction methods to generate additional information concerning the fine scale structure of the solidified materials. The interface between the container and solidified material will be examined critically using optical microscopy and X-Ray microprobe analysis to determine the nature of the interface.

9. ANTICIPATED RESULTS

In the experiments described under general morphology studies (5.1.1 above) it is anticipated that changes in the solid-liquid interfacial energy brought about by changes in the characteristics of the cell liners will produce ultimately differences in the distribution of ullage space. For example, for low relative interfacial energies (wetting) surface tension forces may permit, in the absence of gravity, migration of the liquid test material around the walls of the cell leaving the ullage in the vicinity of the center (Figure 25a). For high relative interfacial energies (nonwetting) the liquid may tend to exist essentially detached from the cell walls (Figure 25b). However, it is conceivable that small perterbations in the LDEF attitude may induce the liquid to break up producing a globular structure with considerable porosity. The complete post flight microstructural analysis of samples should enable flow patterns and flow characteristics generated within the liquid which led to the final structure to be identified.

In the experiments described under Convection Studies (5.1.2 above) radiant heating is used to produce a liquid pool in the center of the "upper" surface of the test sample. It is anticipated that the temperature at the center of the liquid pool will be considerably higher than that at the edge adjacent to the unmelted material. The temperature gradient will change the liquid-vapor interfacial energy locally and induce surface tension driven

convection which should change the profile of the solid-liquid interface. If convection is present then the rate of heat transfer and melting will be increased. The result should be an increase in the maximum diameter of the pool (Figure 25 c,d). Examination of the structure of the sectioned samples will enable the extent of melting in a particular test (solid-liquid interface) to be determined. It is anticipated that the extent of melting due to convection should increase with an increase in time. The position of the solid-liquid interfacial boundaries (profile) determined from post flight specimen examination will be compared with the calculated position of the solid-liquid interfacial boundaries (profile based on a conduction (no convection) model of the melting process). It is hoped that the differences in shapes of the boundaries can be attributed to convection currents in the melt driven by surface tension.

10. WORK PLAN

10.1 Concepts of Work Plan

Early space shuttle missions will involve many widely different experimental packages within each payload. Each of these packages will be conceived, designed, constructed, and tested at sites remote from the National Aeronautics and Space Administration, Langley Research Center. Clearly, it is of the utmost importance that experimental packages arrive at the Center at the prescribed time for the overall success of the mission. A work schedule has been devised to assure efficient utilization of the time, funds, material and personnel resources and to provide the National Aeronautics and Space Administration with an estimate of the time required to produce the proposed experimental package.

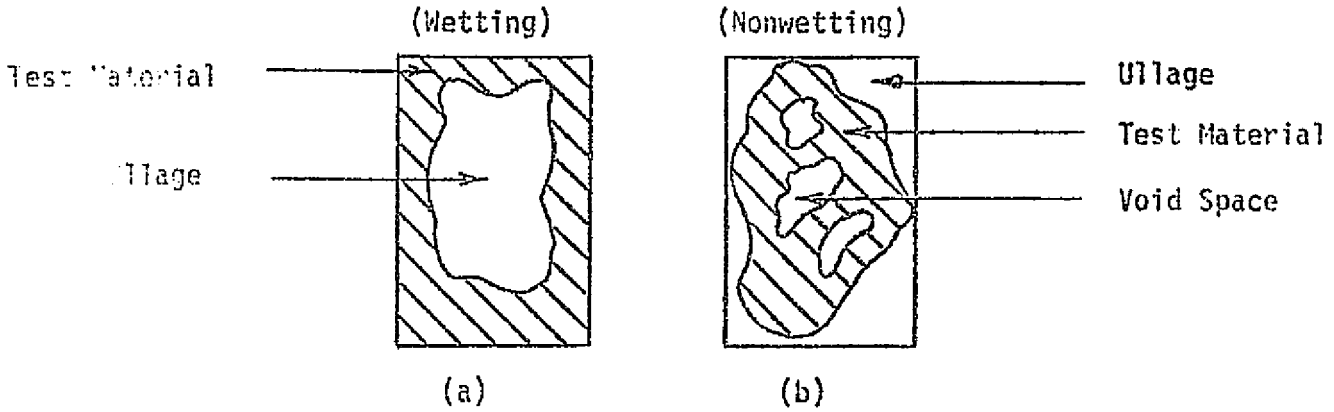

Possible Location of Ullage Space.

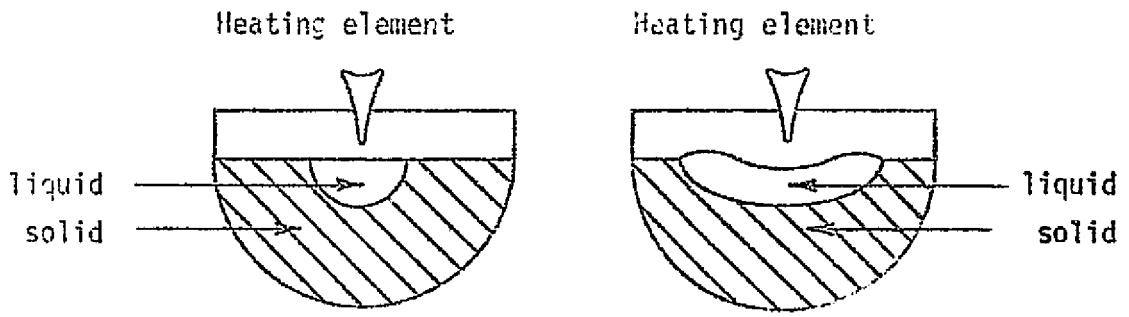

Surface Tension Driven Convection.

FIGURE 25 Location of Ullage Space and Surface Tension Driven Convection

10.2 Management

The limited nature, size and scope of the proposed activity is such that complex managerial arrangements and plans are not required.

Dr. Bailey, Professor of Mechanical and Aerospace Engineering will serve as principal investigator and assume administrative responsibility for the project. He will have responsibility also for sample material selection, fabrication and post flight data analysis. Dr. Whitfield, Professor of Mechanical and Aerospace Engineering will serve as co-principal investigator and assume responsibility for hardware design, development, and testing.

A number of graduate students will assist the principal and co-principal investigators with details of the experimental design, preparation of drawings of hardware, hardware acquisition, testing and data reduction and analysis. It is anticipated that their contributions will form the basis of theses in partial fulfillment of advanced degrees.

10.3 Method of Experiment Acquisition

A number of major tasks associated with the preliminary design of an experiment to study the solidification of materials under a zero gravity environment have completed under the present grant. These tasks include (i) review and critical evaluation of the technical literature, (ii) establishment of contact with NASA personnel having an active interest in the proposed experiment, (iii) establishment of contact with NASA personnel capable of providing most recent information concerning experiment hardware components (power pack, timer systems, etc), and (iv) completion of preliminary design study including selection of design concepts, selection of materials, definition of range of experimental conditions, summary of

thermal, mechanical and physical property data for test and hardware materials and accurate assessment of power requirements.

The initial activity as shown in the Project Schedule, (Figs. 26 and 27) will be the overall design of the major subsystems or modules. Design concepts, including alternative schemes, for the power, timing and heater modules will be developed and submitted to NASA-Langley Research Center for review and approval. After approval of the design concept details of the actual power, timing and heater modules will be developed and again submitted to NASA-Langley Research Center for review and approval. Once approval is obtained, final drawings and detailed specifications will be prepared and submitted for final review and approval. By maintaining close cooperation between NASA-Langley Research Center and North Carolina State University it is believed that suggestions can be easily incorporated into the design and the need for radical changes avoided.

After review of the final drawings and specifications, the experimental package will be fabricated in the Precision Workshop of the Engineering Research Services Division of the School of Engineering at North Carolina State University. Personnel in the workshop have had extensive experience in the fabrication of sophisticated and specialized pieces of research equipment. If a need arises for change in either the design or specifications of the experiment during fabrication then approval will be sought from NASA-Langley Research Center prior to their execution. Concurrent with the fabrication of the experiment detailed test plans and procedures for experiment qualifications will be developed and submitted to NASA-Langley Research Center for approval.

At the present time it is planned to test the experimental package in the Department of Mechanical and Aerospace Engineering at North Carolina

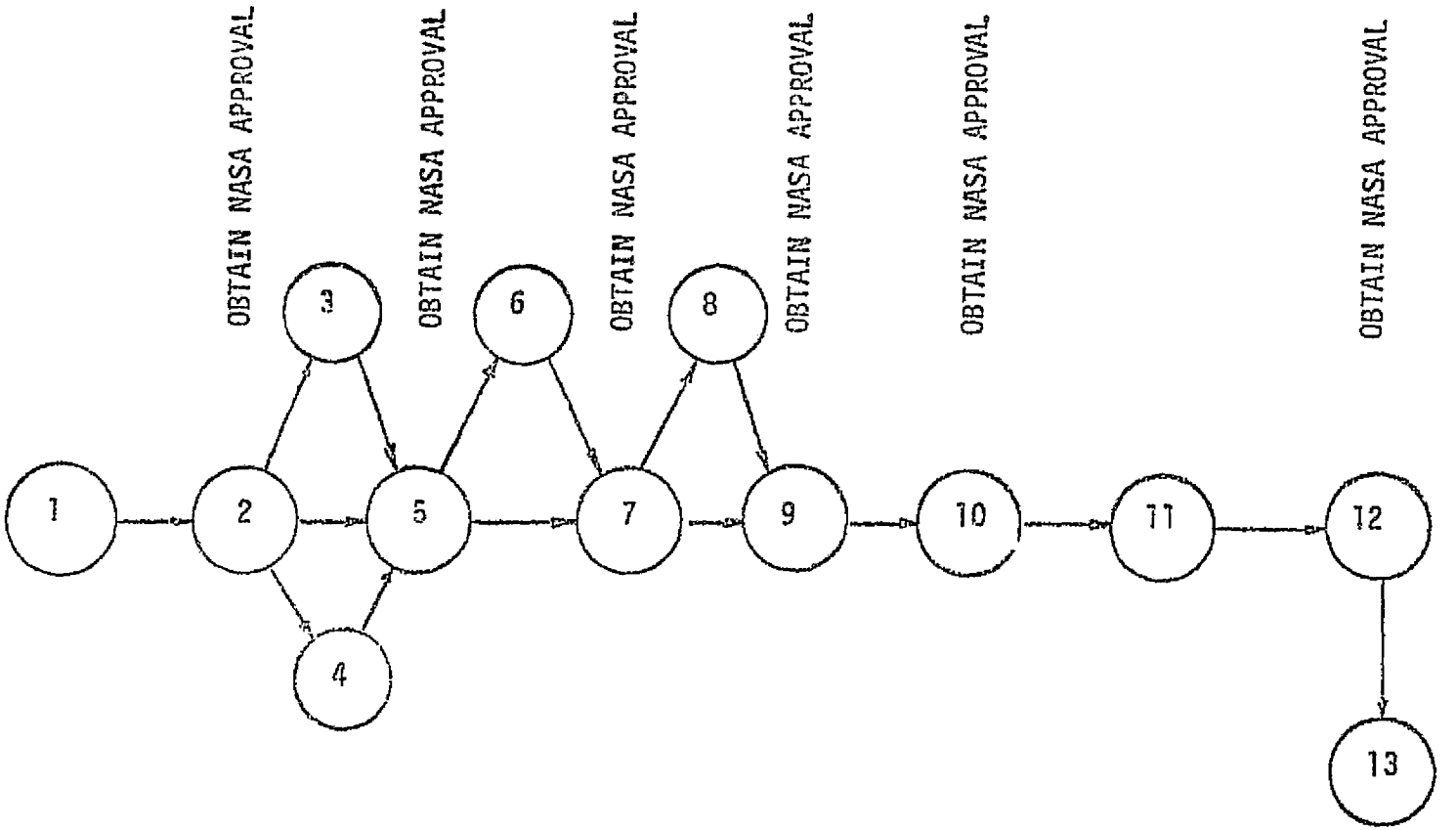

1 Start
2 Overall design complete
3 Detail design of sample module complete
4 Detail design of timer module complete
5 Detail design of power module complete
6 Hardware component procurement complete
7 Final drawings and specifications prepared
8 Test program design complete
9 Experiment fabrication complete
10 Experiment testing complete
11 Test analysis and experiment modification complete
12 Final checkout and modification complete
13 Deliver Experiment to Langley Research Center

FIGURE 26. Project Plan

TASKS	TIME			
	Year One	Year Two	Year Three	Year Four
1. Overall Design of Experiments	XX XX XX XX			
2. Detail Design of Sample Module	XX XX XX XX			
3. Detail Design of Power Module	XX XX XX XX			
4. Detail Design of Timer Module	XX XX XX XX			
5. Hardware Component Procurement	XX XX XX XX			
6. Prepare Final Drawings	XX XX			
7. Fabricate Experiment		XXXX XXXX		
8. Conduct Test Program		XX XX		
9. Test Analysis and Modification		XX XX XX XX		
10. Final Checkout and Calibration		X X X X	X X X X	
11. Deliver Experiment to NASA LaRC			X X X X	
12. NASA Review	X X X X X X X X X	X X X X X X	X X X	
13. Post Flight Analysis				XX XX XX

Project schedule may be expanded or contracted to meet NASA requirements by a change in effort.

FIGURE 27 Project Schedule

State University. Perhaps the most difficult tests to devise are those relating to the extremely high noise levels (~150 Db) and intense vibration to which the experimental package will be exposed during launch. However, the noise and vibration profiles given in the Users Guide have been discussed with Dr. F. D. Hart, Director of the Center for Acoustical Studies at North Carolina State University and he has agreed to assist in the design of a siren to obtain the appropriate noise levels and in the programming of a shaker table to generate the appropriate vibration profile. In addition, the experiment will be tested in the high vacuum system in the Department of Mechanical and Aerospace Engineering. This facility is capable of maintaining an environment of 10^{-8} Torr. After each of the devised tests the experimental package will be tested thoroughly through its complete cycle. It is planned to gather extensive qualification test data and postqualification data of tested experimental package. This data and appropriate analyses will be submitted to NASA-Langley Research Center for approval. It is hoped that NASA-Langley Research Center personnel will be able to visit the University to witness the qualification tests.

At the present time these authors are not aware of any experiments similar to those proposed which are being considered for inclusion of the LDEF mission. However, it is planned to maintain close communication with the LDEF project office so that should such experiments appear, then contact can be made with the appropriate investigator quickly with a view to the establishment of a cooperative effort to avoid possible unnecessary duplication.

Support will be required to integrate the experimental package into the LDEF. However, all that is necessary is to bolt the package to the appropriate tray.

Every effort will be made to assure that the experimental package is safe such that it will not pose any threat to either the shuttle craft or shuttle crew. Wherever possible, age hardened aluminum alloy (6061) and stainless steel will be used as structural materials. In addition, an attempt will be made to select test materials which are chemically inert, nontoxic and noncorrosive. The experimental package itself will be designed to withstand the temperatures, pressures, and mechanical and acoustical vibrations outlined in the LDEF Users Guide with an adequate factor of safety. The test program will verify the reliability of the experimental package to withstand simulated flight conditions. In addition, the experimental package will be sealed in an aluminum alloy container designed to remain intact even under the most severe impact (crash) conditions.

10.4 Facilities and Equipment

As stated above a straightforward engineering design effort is required to select materials and to design the timer and heater/power modules. Familiar, well characterized materials, designs and components will be used. Adequate facilities exist on the campus at North Carolina State University to design, fabricate and test the experimental package. In addition, adequate well known standard diagnostic techniques will be used for post flight data analysis. All necessary equipment for the conduct of the analysis exists also on the campus at North Carolina State University. Equipment or special facilities from NASA and other government agencies is not required.

10.5 Cost Estimation

The completion of an experimental package suitable for flight aboard an early space shuttle mission involves several well defined functions which

TABLE XI. COST ANALYSIS

FUNCTION	ESTIMATED COST
Design	$ 25,000.00
Hardware	12,000.00
Testing	22,000.00
Integration Costs	8,000.00
Data Evaluation	20,000.00
TOTAL COST	$ 87,000.00

include design, hardware testing, integration and data evaluation. A tentative cost analysis based on these categories is given in Table XI.

11. REFERENCES

1. L. L. Lacy and G. H. Otto. "The Behavior of Immiscible Liquids in Space". AIAA Paper No. 74-668, July 1974.

2. J. L. Reger. "Immiscible Alloy Compositions". The third space processing symp. on skylab results. Vol. 1, June 1974, pp. 133-158.

3. A. S. Yue and J. G. Yu. "Halide Eutectic Growth". The third space processing symp. on skylab results. Vol. 1, June 1974, pp. 469-489.

4. A. S. Yue and J. G. Yu. "Solidification of NaCl-NaF Eutectic in Space". AIAA Paper No. 74-646, July 1974.

5. T. Z. Kuttamis, F. C. Douglas, and F. S. Galasso. "Radial and Directional Solidification of Metallic Systems in Space". AIAA Paper No. 74-645, July 1974.

6. M. R. Brashears. "Research Study of Materials Processing in Space Experiment M512". Phase B Report, July 15, 1973.

7. R. T. Frost, E. H. Stockhoff, and G. Wouch. "Electromagnetic Containerless Melting and Solidification in the Weightless Environment". The third space processing symp. on skylab results. Vol. 2, June 1974, pp. 603-646.

8. G. Wouch and H. L. Bloom. "Free Suspension Processing - A Review of Selected User Interests and Requirements". AIAA Paper No. 74-649, July 1974.

9. R. H. Hopkins. "Eutectic Experiment Development for Space Processing". Final Report (Contract NAS8-21905), Jan. 1 - Dec. 1, 1972.

10. F. C. Douglas and F. S. Galasso. "Eutectic Solidification". The third space processing symp. on skylab results. Vol. 2, June 1974.

11. J. P. Doty and J. A. Reising. "Study of Single Crystals of Metal Solid Solutions". Final Report (Contract NAS8-29077), May 21, 1973.

12. J. W. Chi, R. G. Seidensticker, and C. S. Duncan. "Thermal Design and Analysis of Skylab Multipurpose Furnace and Experiments". AIAA Paper No. 74-650, July 1974.

13. C. J. Smithells. "Metals Reference Book". New York Plenum Press, London Butterworths, Vol. 1, 2, and 3, Fourth Edition, 1967.

14. American Petroleum Institute Research Project 44. "Selected Physical and Thermodynamic Properties of Hydrocarbons and Related Compounds". Collage Station, Texas: Texas A & M University, 1959 - Kept-to-date.

15. T. Goodman. "The Heat Balance Integral and Its Application to Problems Involving Change of Phase". Trans. Am. Soc. Mech. Engr. 80, 335-342, 1958.

16. J. A. Duffie and W. A. Beckman. "Solar Energy Thermal Processes". Wiley Interscience, New York, 1974.